Arabian Journal of Chemistry (2023) **16**, 104514

King Saud University

Arabian Journal of Chemistry

www.ksu.edu.sa
www.sciencedirect.com

ORIGINAL ARTICLE

1-Benzamido-1,4-dihydropyridine derivatives as anticancer agents: *in vitro* and *in vivo* assays

Sandra Ardevines [a], Fernando Auria-Luna [a], Eduardo Romanos [a,b,c], Vanesa Fernández-Moreira [b], Andrea Benedi [d], M. Concepción Gimeno [b], Isabel Marzo [d], Eugenia Marqués-López [a,*], Raquel P. Herrera [a,*]

[a] *Laboratorio de Organocatálisis Asimétrica, Departamento de Química Orgánica. Instituto de Síntesis Química y Catálisis Homogénea (ISQCH), CSIC-Universidad de Zaragoza, C/ Pedro Cerbuna 12, E-50009 Zaragoza, Spain*
[b] *Departamento de Química Inorgánica. Instituto de Síntesis Química y Catálisis Homogénea (ISQCH), CSIC-Universidad de Zaragoza, C/ Pedro Cerbuna 12, E-50009 Zaragoza, Spain*
[c] *Departamento de Imagen y Fenotipado, Instituto Aragonés de Ciencias de la Salud. Centro de Investigación Biomédica de Aragón (CIBA), Avda. San Juan Bosco, 13, planta D, E-50009 Zaragoza, Spain*
[d] *Departamento de Bioquímica y Biología Molecular y Celular, Universidad de Zaragoza, C/ Pedro Cerbuna 12, E-50009 Zaragoza, Spain*

Received 5 September 2022; accepted 7 December 2022
Available online 12 December 2022

KEYWORDS

Cancer;
Hydrazide;
1,4-Dihydropyridine;
In vitro;
In vivo (mice);
Paraptosis

Abstract 1,4-Dihydropyridine is a privileged scaffold present in many bioactive molecules, from coenzymes to commercially available drugs. Among other interesting properties, it has been found good anticancer activity in some of these 1,4-DHPs, therefore many research groups are trying to develop new compounds based on this structural core.

For this purpose, in this work, a family of 23 new 1,4-dihydropyridines has been synthesized using hydrazide and malononitrile derivatives as precursors. This straightforward catalytic process has given rise to the desired products with moderate to excellent yields. All the compounds have been tested against four different cancer cell lines [HeLa (human cervical carcinoma), Jurkat (leukemia), A549 (human lung cancer) and MIA PaCa-2 (pancreatic cancer)] to establish a preliminary structure–activity relationship. From this study, and among the best candidates, we chose 4-chlorophenyl and 4-(trifluoromethyl)phenyl derivatives in the malononitrile ring to synthesize a second generation of molecules with enhanced cytotoxicity, modifying the substituent in the *N*-heterocyclic position (acylhydrazine moieties). With this second generation of compounds, we successfully decreased the IC_{50} until 7 μM.

* Corresponding authors.
E-mail addresses: mmaamarq@unizar.es (E. Marqués-López), raquelph@unizar.es (R.P. Herrera).
Peer review under responsibility of King Saud University.

Production and hosting by Elsevier

https://doi.org/10.1016/j.arabjc.2022.104514

An in-depth analysis of their biological properties suggests that these promising compounds trigger a non-conventional cell death mechanism known as paraptosis. Moreover, the tested photophysical properties of these products show in some cases an interesting long wavelength emission and excitation, potentially leading to new biosensors or theragnostic agents.

Finally, *in vivo* assays concerning the acute toxicity in mice of two of the most active compounds (with an alkyl chain of seven carbon atoms in the acylhydrazine moiety) demonstrated that even dosed at thousands fold the corresponding IC_{50} values (2500 and 3300 times more concentrated than the IC_{50} values for the two compounds studied), there was no sign of harmful effects on the tested subjects, results that support their use in further studies to discover new anticancer drugs.

1. Introduction

The 1,4-dihydropyridine (1,4-DHP) core is present in many versatile synthetic intermediates giving access to biologically active targets (Edraki et al., 2009; Carosati et al., 2012; Dhinakaran et al., 2015; Sharma and Singh, 2017). The first appearance in synthetic chemistry of these structures came with the pioneering work of Arthur Hantzsch and his method for the synthesis of pyridines in 1881 (Hantzsch, 1881). However, it was not until the mid-1970s when the activity of molecules containing this structural moiety such as nifedipine, a well-known antihypertensive agent used in the treatment of cardiovascular diseases, was discovered (Fig. 1) (Loev et al., 1974). Since then, many other potential structures have been developed and commercialized as excellent calcium channel blockers (Safak and Simsek, 2006; Ioan et al., 2011; Bruncko, 2012). Moreover, further studies have shown that 1,4-DHP derivatives can also exhibit relevant anti-inflammatory (Idhayadhulla et al., 2015; Indumathi et al., 2015), antimicrobial (Chhillar et al., 2006; Sirisha et al., 2010; Sirisha et al., 2011; Mehta and Verma, 2013; Olejníková et al., 2014), anticonvulsant (Hadizadeh et al., 2013; Ramírez-San Juan et al., 2014), analgesic (Gadotti et al., 2015), anti-HIV (Hilgeroth, 2002) or antioxidant (Milkovic et al., 2018) activity, among others.

1,4-Dihydropyridines are also systems of crucial importance due to their presence in the core of biologically relevant molecules such as cofactors NADH and NADPH (Pollak et al., 2007; Griendling et al., 1994; Liu et al., 2002). Therefore, the involvement of these compounds in many biological processes has turned them into potential therapeutic targets of great interest in medicinal chemistry (Reddy et al., 2007; Mai et al., 2009; Sharma and Singh, 2017; Talwan et al., 2017).

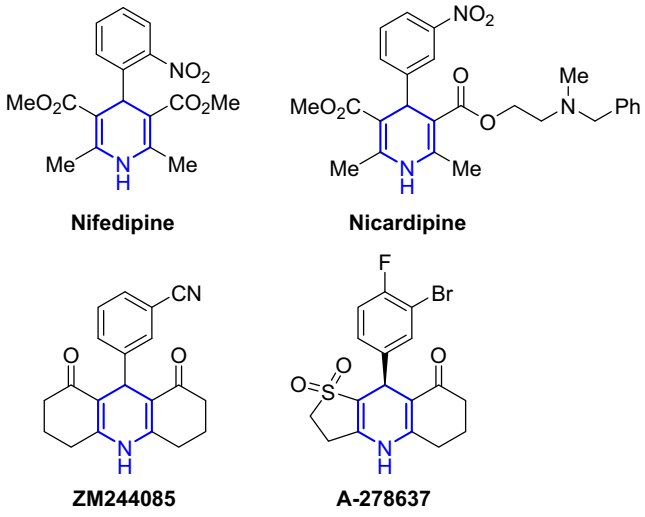

Fig. 1 Structures of biologically active 1,4-dihydropyridines.

Because of this wide variety of pharmacological properties, a good number of studies on the synthesis of this type of compounds have been carried out during the last decades, making it an active and highly relevant field of research these days (Saini et al., 2008; Wan and Liu, 2012; Pham et al., 2012).

In the context of our own research, we have lately described important approaches focused on the development of new enantioenriched 1,4-DHPs, becoming some of the few reported examples in this field to date (Auria-Luna et al., 2015, 2017, 2018). More recently, in our search for new potential anticancer agents (Fernández-Moreira et al., 2016, 2019a,b; Goitia et al., 2013; Gutiérrez et al., 2014, 2015; Montanel-Pérez et al., 2015; Ortego et al., 2016; Quintana et al., 2016; Salvador-Gil et al., 2017), we have also published an interesting work using new 1,4-DHPs with potential theragnostic properties (Auria-Luna et al., 2020).

It is also worth mentioning that 1,4-dihydropyridines have also been explored as antitumoral agents (Voigt et al., 2007; Shekari et al., 2015) because of the importance of this illness as one of the leading causes of death in the world today (Bray et al., 2021; World, 2021). The treatment of cancer has attracted the efforts of many scientific groups with the main goal of decreasing the growth of tumor cells avoiding side effects or reducing them to improve the patient's quality of life and survival (Alexiou et al., 2006; Bruijnincx and Sadler, 2008; Salari et al., 2022; Cuciniello et al., 2021; Prabahar et al., 2021; Dhankhar et al., 2021). Concerning the use of 1,4-DHPs as anticancer agents, these have been less explored, and the only cases reported so far have been using (1*H*)-dihydropyridines (Morshed et al., 2005; Bazargan et al., 2008; Abbas et al., 2010; Firuzi et al., 2013; Azzam and Mohareb, 2015; Gómez-Galeno et al., 2018; Goto et al., 2018), maybe by similitude with NADH. In this sense, our recent results are pioneering, as we have demonstrated that *N*-phenyl-1,4-dihydropyridines and their ureido derivatives could also show potent anticancer activity, achieving competitive results in comparison with those previously reported in the literature (Auria-Luna et al., 2020). Moreover, designing these compounds bearing luminescent fragments will allow us to find out the biodistribution of the molecules within the tumor cells (Fernández-Moreira et al., 2014; Fernández-Moreira and Gimeno, 2018; Fernández-Moreira and Sastre-Martín, 2017; Luengo et al., 2017; Visbal et al., 2016).

All these interesting properties make 1,4-DHP derivatives crucial leads in the ongoing search for new drug candidates and an appealing target for new effective cancer therapies. Therefore, herein we describe a pioneering study using 23 new 1-benzamido-1,4-dihydropyridine derivatives with potential bioactive properties. The toxicity of this new family of compounds has been evaluated against four different cancer cell lines: HeLa (human cervical carcinoma), Jurkat (leukemia), A549 (human lung cancer) and MIA PaCa-2 (pancreatic cancer). Additional biological assays have been performed to obtain informa-

tion regarding the mechanism of cellular death associated with the compounds. Further photophysical properties have been analyzed to evaluate these compounds as plausible theragnostic agents. Finally, the best candidates were also analyzed in *in vivo* toxicity assays to establish the way for a future efficacy study with the ultimate aim of discovering new potential anticancer drugs.

2. Materials and methods

2.1. Chemistry and photophysics. General experimental methods and instrumentation

All commercial reagents and solvents were used without prior purification.

Analytical thin-layer chromatography was performed on 0.25 mm silica gel 60-F plates. ESI ionization method and MicroTof-Q Bruker mass analyzer were used for the HRMS measurements. NMR spectroscopy was conducted using Bruker ARX300, AV300 or AV400 spectrometers. ^{1}H NMR spectra were recorded at 300 or 400 MHz, and ^{13}C{^{1}H}-APT NMR spectra were recorded at 75 or 100 MHz, using DMSO-d_6 as the deuterated solvent. Chemical shifts were reported in the δ scale relative to residual DMSO (2.50 ppm) for ^{1}H NMR and to the central line of DMSO-d_6 (39.52 ppm) for ^{13}C {^{1}H}-APT NMR.

Room temperature steady-state emission and excitation spectra were recorded in DMSO solution with a Jobin-Yvon-Horiba Fluorolog FL3-11 spectrometer.

2.2. General procedure for the synthesis of 1,4-DHP derivatives 7

Hydrazone **3a-g** (0.5 mmol) is weighed and solved in 2 mL of methanol (for **3a**) or ethanol (for **3b-g**). Then, an excess of the precursor **6a-k** (0.6 mmol) is added and Et_3N (20 mol%, 14 μL) is incorporated. The reaction mixture is stirred at room temperature for 24 h. Then, precipitating the reaction crude with hexane, filtering the solid under vacuum, and washing successively with the same solvent, allowed to isolate the corresponding DHP with high purity.

*2.2.1. Dimethyl 6-amino-1-benzamido-5-cyano-4-phenyl-1,4-dihydropyridine-2,3-dicarboxylate (**7aa**)*

Following the general procedure, compound **7aa** was obtained as a pale-yellow solid in 85 % yield (184.7 mg). ^{1}H NMR (300 MHz, DMSO-d_6) δ 3.51 (br s, 3H), 3.64 (br s, 3H), 4.36 (s, 0.7H), 4.47 (br s, 0.3H), 6.31 (s, 1.5H), 6.46 (s, 0.5H), 7.24 (t, J = 7.3 Hz, 1.5H Ar), 7.35 (t, J = 7.1 Hz, 2H Ar), 7.53 (t, J = 7.1 Hz, 3H Ar), 7.63 (t, J = 7.1 Hz, 1.5H Ar), 7.78–7.90 (m, 2H Ar), 11.23 (br s, 0.7H), 11.33 (br s, 0.3H). ^{13}C{^{1}H}-APT NMR (75 MHz, DMSO-d_6) δ 51.9 (1C), 52.8 (1C), 58.5 (1C), 104.6 (1C), 120.9 (1C), 126.9 (1C), 127.7 (2C), 127.9 (2C), 128.4 (2C), 128.5 (2C), 131.3 (1C), 132.5 (1C), 142.6 (1C), 145.7 (1C), 151.2 (1C), 162.5 (1C), 164.7 (1C), 166.3 (1C), 166.7 (1C). IR (neat) (cm^{-1}) IR (neat) (cm^{-1}) 3671, 3412, 3334, 3247, 2190, 1717, 1685, 1662, 1590, 1477, 1433, 1375, 1336, 1302, 1231, 1187, 1120, 1076, 1066, 1038, 1028, 944, 767, 710, 698, 687. HRMS (ESI +) calculated for $C_{23}H_{20}N_4NaO_5$ 455.1326; found 455.1326 [M + Na]$^{+}$.

*2.2.2. Diethyl 6-amino-1-benzamido-5-cyano-4-phenyl-1,4-dihydropyridine-2,3-dicarboxylate (**7ba**)*

Following the general procedure, compound **7ba** was obtained as a white solid in 19 % yield (44.4 mg). ^{1}H NMR (400 MHz, DMSO-d_6) δ 0.95–1.08 (m, 6H), 3.89–4.00 (m, 2H), 4.01–4.14 (m, 2H), 4.36 (s, 0.7H), 4.48 (s, 0.3H), 6.39 (s, 1.5H), 6.44 (br s, 0.5H), 7.19–7.28 (m, 1.5H Ar), 7.31–7.40 (m, 2H Ar), 7.46–7.67 (m, 4.5H Ar), 7.81–7.94 (m, 2H Ar), 11.23 (s, 0.7H), 11.34 (br s, 0.3H). ^{13}C{^{1}H}-APT NMR (100 MHz, DMSO-d_6) δ 13.5 (1C), 13.7 (1C), 39.3 (1C), 60.4 (1C), 61.8 (1C), 104.7 (1C), 121.0 (1C), 126.8 (1C), 127.2 (2C), 127.9 (2C), 128.2 (2C), 128.5 (2C), 131.2 (1C), 132.6 (1C), 142.5 (1C), 145.8 (1C), 151.2 (1C), 161.9 (1C), 164.2 (1C), 165.9 (1C), 166.5 (1C). IR (neat) (cm^{-1}) 3662, 3429, 3344, 3221, 2987, 2901, 2184, 1932, 1729, 1704, 1663, 1594, 1506, 1479, 1427, 1393, 1374, 1299, 1269, 1250, 1218, 1103, 1075, 1066, 1057, 1028, 891, 863, 714, 699, 688. HRMS (ESI +) calculated for $C_{25}H_{24}N_4NaO_5$ 483.1639; found 483.1639 [M + Na]$^{+}$.

*2.2.3. Diethyl 6-amino-1-benzamido-5-cyano-4-(naphthalen-1-yl)-1,4-dihydropyridine-2,3-dicarboxylate (**7bb**)*

Following the general procedure, compound **7bb** was obtained as a pale-yellow solid in 83 % yield (212.4 mg). ^{1}H NMR (400 MHz, DMSO-d_6) δ 0.66 (t, J = 0.7 Hz, 0.8H), 0.72 (t, J = 0.7 Hz, 1.9H), 0.99 (t, J = 1.0 Hz, 0.9H), 1.05 (t, J = 1.0 Hz, 1.9H), 3.67–3.82 (m, 2H), 3.96–4.19 (m, 2H), 5.42 (br s, 0.7H), 5.48 (br s, 0.3H), 6.33 (s, 1.5H), 6.37 (br s, 0.5H), 7.41–7.68 (m, 6H Ar), 7.78–7.97 (m, 4H Ar), 8.11 (d, J = 8.1 Hz, 1H Ar), 8.38–8.50 (m, 1H Ar), 11.28 (s, 0.7H), 11.39 (s, 0.3H). ^{13}C{^{1}H}-APT NMR (100 MHz, DMSO-d_6) δ 13.5 (1C), 13.4 (1C), 59.1 (1C), 60.2 (1C), 61.8 (1C), 105.6 (1C), 120.9 (1C), 123.7 (1C), 125.5 (1C), 125.9 (1C), 126.1 (1C), 127.0 (1C), 127.2 (1C), 127.9 (1C), 128.2 (1C), 128.3 (1C), 128.5 (1C), 130.4 (1C), 131.2 (1C), 132.6 (1C), 133.0 (1C), 142.9 (1C), 151.1 (1C), 162.0 (1C), 164.2 (1C), 166.5 (1C). IR (neat) (cm^{-1}) 3684, 3662, 3421, 3345, 3221, 2988, 2901, 2181, 1933, 1722, 1701, 1681, 1661, 1593, 1508, 1475, 1407, 1393, 1376, 1263, 1241, 1103, 1075, 1066, 1057, 1027, 892, 864, 775, 712, 680. HRMS (ESI +) calculated for $C_{29}H_{26}N_4NaO_5$ 533.1795; found 533.1793 [M + Na]$^{+}$.

*2.2.4. Diethyl 6-amino-1-benzamido-5-cyano-4-(thiophen-2-yl)-1,4-dihydropyridine-2,3-dicarboxylate (**7bc**)*

Following the general procedure, compound **7bc** was obtained as a dark brown solid in 40 % yield (93.3 mg). ^{1}H NMR (400 MHz, DMSO-d_6) δ 0.93–1.22 (m, 6H), 3.94–4.17 (m, 4H), 4.66 (s, 0.6H), 4.83 (s, 0.4H), 6.49 (s, 1.2H), 6.56 (s, 0.8H), 7.31–8.02 (m, 8H Ar), 11.22 (s, 0.6H), 11.39 (s, 0.4H). ^{13}C{^{1}H}-APT NMR (100 MHz, DMSO-d_6) δ 13.5 (1C), 13.8 (1C), 33.7 (1C), 60.6 (1C), 61.8 (1C), 104.3 (1C), 117.5 (1C), 120.9 (1C), 124.5 (1C), 125.0 (1C), 127.1 (1C), 127.9 (1C), 128.4 (1C), 131.2 (1C), 132.1 (1C), 142.2 (1C), 145.9 (1C), 148.8 (1C), 151.3 (1C), 161.7 (1C), 164.0 (1C), 166.0 (1C). IR (neat) (cm^{-1}) 3685, 3674, 3423, 3314, 3200, 2987, 2901, 2226, 2189, 1934, 1731, 1708, 1660, 1578, 1506, 1479, 1450, 1434, 1406, 1393, 1382, 1249, 1229, 1066, 1057, 1028, 892, 879, 867, 708, 690. HRMS (ESI +) calculated for $C_{23}H_{22}N_4NaO_5S$ 489.1203; found 489.1199 [M + Na]$^{+}$.

*2.2.5. Diethyl 6-amino-1-benzamido-5-cyano-4-(3-nitrophenyl)-1,4-dihydropyridine-2,3-dicarboxylate (**7bd**)*

Following the general procedure, compound **7bd** was obtained as a pale-brown solid in 92 % yield (233.8 mg). ^{1}H NMR (300 MHz, DMSO-d_6) δ 0.93–1.13 (m, 6H), 3.84–4.02 (m, 2H), 4.03–4.22 (m, 2H), 4.62 (s, 0.75H), 4.76 (s, 0.25H), 6.59 (br s, 1.5H), 6.66 (br s, 0.5H), 7.47–7.77 (m, 4.5H Ar), 7.83–7.95 (m, 2H Ar), 8.04–8.21 (m, 2H Ar), 8.33 (s, 0.5H Ar), 11.33 (s, 0.75H), 11.44 (br s, 0.25H). ^{13}C{^{1}H}-APT NMR (75 MHz, DMSO-d_6) δ 13.5 (1C), 13.6 (1C), 39.2 (1C), 60.7 (1C), 61.9 (1C), 104.1 (1C), 120.6 (1C), 122.0 (1C), 122.3 (1C), 128.0 (2C), 128.5 (2C), 130.1 (1C), 131.0 (1C), 132.6 (1C), 134.9 (1C), 143.2 (1C), 147.7 (1C), 148.1 (1C), 151.7 (1C), 151.9 (1C), 161.7 (1C), 163.9 (1C), 166.6 (1C). IR (neat) (cm^{-1}) 3685, 3661, 3413, 3339, 3249, 3218, 2987, 2901, 2181, 1922, 1725, 1702, 1681, 1663, 1589, 1530, 1505, 1475, 1433, 1405, 1394, 1377, 1345, 1324, 1300, 1268, 1250, 1231, 1107, 1066, 1057, 1027, 897, 879, 866, 811, 733, 718, 703, 688. HRMS (ESI+) calculated for $C_{25}H_{23}N_5NaO_7$ 528.1490; found 528.1486 [M + Na]$^+$.

*2.2.6. Diethyl 6-amino-1-benzamido-4-(3-chlorophenyl)-5-cyano-1,4-dihydropyridine-2,3-dicarboxylate (**7be**)*

Following the general procedure, compound **7be** was obtained as a white solid in 89 % yield (221.1 mg). ^{1}H NMR (300 MHz, DMSO-d_6) δ 0.92–1.09 (m, 6H), 3.88–4.16 (m, 4H), 4.40 (s, 0.75H), 4.52 (s, 0.25H), 6.48 (s, 1.5H), 6.55 (br s, 0.5H), 7.17–7.44 (m, 2.5H Ar), 7.46–7.67 (m, 4.5H Ar), 7.80–7.93 (m, 2H Ar), 11.26 (s, 0.75H), 11.36 (s, 0.25H). ^{13}C{^{1}H}-APT NMR (75 MHz, DMSO-d_6) δ 13.5 (1C), 13.7 (1C), 39.2 (1C), 60.6 (1C), 61.9 (1C), 104.3 (1C), 120.7 (1C), 126.0 (1C), 126.7 (1C), 126.9 (1C), 128.0 (2C), 128.4 (1C), 128.5 (2C), 130.1 (1C), 131.1 (1C), 132.6 (1C), 133.0 (1C), 142.8 (1C), 148.3 (1C), 151.4 (1C), 161.8 (1C), 164.0 (1C), 166.6 (1C). IR (neat) (cm^{-1}) 3685, 3662, 3420, 3336, 3222, 2987, 2901, 2184, 1932, 1727, 1703, 1662, 1590, 1505, 1475, 1428, 1406, 1393, 1378, 1349, 1325, 1298, 1249, 1241, 1103, 1076, 1066, 1057, 1028, 892, 870, 789, 770, 713, 695, 687. HRMS (ESI+) calculated for $C_{25}H_{23}ClN_4NaO_5$ 517.1249; found 517.1249 [M + Na]$^+$.

*2.2.7. Diethyl 6-amino-1-benzamido-5-cyano-4-(4-nitrophenyl)-1,4-dihydropyridine-2,3-dicarboxylate (**7bf**)*

Following the general procedure, compound **7bf** was obtained as a brown solid in 96 % yield (241.9 mg). ^{1}H NMR (300 MHz, DMSO-d_6) δ 0.89–1.13 (m, 6H), 3.82–4.21 (m, 4H), 4.57 (s, 1H), 6.57 (s, 2H), 7.37–8.02 (m, 7H Ar), 8.12–8.28 (m, 2H Ar), 11.31 (br s, 1H). ^{13}C{^{1}H}-APT NMR (75 MHz, DMSO-d_6) δ 13.5 (1C), 13.7 (1C), 45.8 (1C), 60.6 (1C), 61.9 (1C), 103.8 (1C), 116.5 (1C), 120.6 (1C), 123.7 (1C), 128.0 (2C), 128.5 (2C), 128.9 (2C), 131.1 (1C), 132.6 (2C), 146.5 (1C), 151.7 (1C), 153.1 (1C), 161.2 (1C), 163.8 (1C), 165.9 (1C), 166.6 (1C). IR (neat) (cm^{-1}) 3674, 3449, 3330, 3201, 2987, 2901, 2184, 1933, 1737, 1704, 1653, 1580, 1515, 1475, 1406, 1393, 1373, 1345, 1305, 1249, 1241, 1226, 1103, 1066, 1057, 1027, 892, 859, 822, 692. HRMS (ESI+) calculated for $C_{25}H_{23}N_5NaO_7$ 528.1490; found 528.1492 [M + Na]$^+$.

*2.2.8. Diethyl 6-amino-1-benzamido-4-(4-chlorophenyl)-5-cyano-1,4-dihydropyridine-2,3-dicarboxylate (**7bg**)*

Following the general procedure, compound **7bg** was obtained as a pale-pink solid in 80 % yield (197.9 mg). ^{1}H NMR (300 MHz, DMSO-d_6) δ 0.92–1.10 (m. 6H), 3.87–4.16 (m, 4H), 4.39 (s, 0.75H), 4.51 (s, 0.25H), 7.20–7.28 (m, 0.5H Ar), 7.37–7.67 (m, 6.5H Ar), 7.81–7.93 (m, 2H Ar), 11.26 (s, 0.75H), 11.35 (br s, 0.25H). ^{13}C{^{1}H}-APT NMR (75 MHz, DMSO-d_6) δ 13.5 (1C), 13.7 (1C), 38.7 (1C), 60.5 (1C), 61.8 (1C), 104.4 (1C), 120.8 (1C), 127.9 (1C), 128.3 (2C), 128.5 (2C), 129.7 (2C), 131.1 (1C), 131.5 (1C), 132.6 (2C), 142.7 (1C), 144.8 (1C), 151.3 (1C), 161.3 (1C), 164.0 (1C), 165.8 (1C), 167.0 (1C). IR (neat) (cm^{-1}) 3685, 3674, 3419, 3329, 3204, 2987, 2901, 2184, 1933, 1704, 1653, 1580, 1510, 1488, 1407, 1393, 1372, 1304, 1249, 1241, 1225, 1066, 1057, 1027, 892, 865, 836, 712, 690. HRMS (ESI+) calculated for $C_{25}H_{23}ClN_4NaO_5$ 517.1249; found 517.1254 [M + Na]$^+$.

*2.2.9. Diethyl 6-amino-1-benzamido-4-(4-bromophenyl)-5-cyano-1,4-dihydropyridine-2,3-dicarboxylate (**7bh**)*

Following the general procedure, compound **7bh** was obtained as a pale-yellow solid in 74 % yield (198.8 mg). ^{1}H NMR (300 MHz, DMSO-d_6) δ 0.93–1.10 (m, 6H), 3.87–4.17 (m, 4H), 4.38 (s, 0.75H), 4.50 (s, 0.25H), 6.46 (s, 1.5H), 6.52 (br s, 0.5H), 7.19 (d, J = 7.2 Hz, 0.5H Ar), 7.45–7.67 (m, 6.5H Ar), 7.81–7.94 (m, 2H Ar), 11.27 (s, 0.75H), 11.35 (br s, 0.25H). ^{13}C{^{1}H}-APT NMR (75 MHz, DMSO-d_6) δ 13.5 (1C), 13.7 (1C), 38.7 (1C), 60.5 (1C), 61.8 (1C), 104.3 (1C), 120.0 (1C), 120.8 (1C), 127.9 (1C), 128.5 (1C), 129.4 (1C), 130.1 (1C), 131.1 (1C), 131.2 (1C), 131.4 (1C), 132.6 (1C), 142.8 (1C), 143.2 (1C), 145.2 (1C), 151.3 (1C), 151.7 (1C), 161.8 (1C), 164.0 (1C), 165.6 (1C), 166.5 (1C). IR (neat) (cm^{-1}) 3685, 3672, 3443, 3261, 3224, 3190, 2987, 2901, 2183, 1934, 1717, 1655, 1579, 1512, 1484, 1435, 1406, 1393, 1383, 1371, 1327, 1310, 1221, 1074, 1066, 1057, 1027, 892, 863, 833, 744, 684. HRMS (ESI+) calculated for $C_{25}H_{24}BrN_4O_5$ 539.0925; found 539.0925 [M + H]$^+$.

*2.2.10. Dimethyl 6-amino-1-benzamido-5-cyano-4-(4-cyanophenyl)-1,4-dihydropyridine-2,3-dicarboxylate (**7ai**)*

Following the general procedure, compound **7ai** was obtained as a pale-yellow solid in 96 % yield (220.0 mg). ^{1}H NMR (400 MHz, DMSO-d_6) δ 3.51 (s, 3H), 3.64 (s, 3H), 4.49 (br s, 1H), 6.55 (s, 2H), 7.39–8.05 (m, 9H Ar), 11.29 (br s, 1H). ^{13}C{^{1}H}-APT NMR (100 MHz, DMSO-d_6) δ 39.3 (1C), 52.0 (1C), 52.9 (1C), 103.9 (1C), 109.8 (1C), 118.9 (1C), 120.5 (1C), 127.9 (1C), 128.5 (4C), 131.2 (1C), 132.6 (4C), 141.1 (1C), 143.3 (1C), 150.9 (1C), 151.5 (1C), 162.2 (1C), 164.4 (1C), 166.8 (1C). IR (neat) (cm^{-1}) 3685, 3673, 3412, 3328, 3206, 2987, 2901, 2231, 2191, 1933, 1750, 1704, 1666, 1589, 1505, 1485, 1432, 1407, 1394, 1382, 1361, 1334, 1300, 1271, 1251, 1242, 1225, 1103, 1066, 1057, 929, 891, 867, 847, 717, 686. HRMS (ESI+) calculated for $C_{24}H_{19}N_5NaO_5$ 480.1278; found 480.1278 [M + Na]$^+$.

*2.2.11. Diethyl 6-amino-1-benzamido-5-cyano-4-(4-cyanophenyl)-1,4-dihydropyridine-2,3-dicarboxylate (**7bi**)*

Following the general procedure, compound **7bi** was obtained as a brown solid in 91 % yield (220.8 mg). ^{1}H NMR

(300 MHz, DMSO-d_6) δ 0.96–1.13 (m, 6H), 3.98 (q, J = 7.1 Hz, 2H), 4.03–4.24 (m, 2H), 4.52 (s, 0.75H), 4.64 (s, 0.25H), 6.53 (s, 1.5H), 6.59 (br s, 0.5H), 7.40–7.98 (m, 9H Ar), 11.31 (s, 0.75H), 11.38 (br s, 0.25H). $^{13}C\{^1H\}$-APT NMR (75 MHz, DMSO-d_6) δ 12.3 (1C), 13.9 (1C), 39.8 (1C), 60.8 (1C), 62.1 (1C), 103.7 (1C), 104.2 (1C), 110.0 (1C), 119.2 (1C), 120.8 (1C), 128.2 (1C), 128.7 (2C), 129.0 (2C), 131.3 (1C), 132.7 (2C), 132.9 (2C), 143.4 (1C), 151.3 (1C), 151.7 (1C), 161.9 (1C), 164.1 (1C), 166.8 (1C). IR (neat) (cm^{-1}) 3685, 3672, 3444, 3274, 3224, 3191, 2987, 2901, 2232, 2183, 1932, 1727, 1713, 1675, 1659, 1577, 1504, 1483, 1437, 1406, 1393, 1382, 1321, 1255, 1227, 1076, 1066, 1057, 892, 880, 862, 847, 768, 684. HRMS (ESI+) calculated for $C_{26}H_{23}N_5NaO_5$ 508.1591; found 508.1569 $[M + Na]^+$.

*2.2.12. Diethyl 6-amino-1-benzamido-5-cyano-4-(p-tolyl)-1,4-dihydropyridine-2,3-dicarboxylate (**7bj**)*

Following the general procedure, compound **7bj** was obtained as a white solid in 92 % yield (218.6 mg). ^1H NMR (400 MHz, DMSO-d_6) δ 1.01–1.22 (m, 6H), 2.33–2.42 (m, 3H), 3.96–4.10 (m, 2.5H), 4.11–4.15 (m, 1.5H), 4.41 (s, 0.7H), 4.53 (s, 0.3H), 6.42 (s, 1.5H), 6.48 (s, 0.5H), 7.16–7.29 (m, 2.5H Ar), 7.49–7.56 (m, 1.5H Ar), 7.57–7.66 (m, 2H Ar), 7.67–7.76 (m, 1H Ar), 7.90–8.04 (m, 2H Ar), 11.28 (s, 0.7H), 11.41 (s, 0.3H). $^{13}C\{^1H\}$-APT NMR (100 MHz, DMSO-d_6) δ 13.5 (1C), 13.7 (1C), 20.7 (1C), 38.8 (1C), 60.4 (1C), 61.7 (1C), 104.8 (1C), 121.0 (1C), 127.1 (1C), 127.8 (1C), 127.9 (1C), 128.3 (1C), 128.4 (1C), 128.8 (1C), 130.2 (1C), 130.7 (1C), 131.2 (1C), 132.5 (1C), 135.9 (1C), 142.3 (1C), 142.9 (1C), 145.7 (1C), 151.2 (1C), 162.0 (1C), 164.2 (1C), 166.4 (1C). IR (neat) (cm^{-1}) 3672, 3435, 3349, 3248, 3220, 2987, 2981, 2901, 2185, 1932, 1731, 1706, 1665, 1594, 1509, 1478, 1428, 1407, 1393, 1373, 1296, 1267, 1250, 1215, 1098, 1077, 1065, 1057, 1027, 880, 860, 803, 714, 687. HRMS (ESI+) calculated for $C_{26}H_{26}N_4NaO_5$ 497.1795; found 497.1799 $[M + Na]^+$.

*2.2.13. Diethyl 6-amino-1-benzamido-5-cyano-4-(4-(trifluoromethyl)phenyl)-1,4-dihydropyridine-2,3-dicarboxylate (**7bk**)*

Following the general procedure, compound **7bk** was obtained as a brown solid in 96 % yield (254.5 mg). ^1H NMR (300 MHz, DMSO-d_6) δ 0.86–1.07 (m, 6H), 3.92 (q, J = 7.2 Hz, 2H), 3.97–4.17 (m, 2H), 4.47 (s, 0.75H), 4.59 (s, 0.25H), 6.48 (s, 1.5H), 6.54 (s, 0.5H), 7.34–7.97 (m, 9H Ar), 11.27 (s, 0.75H), 11.35 (br s, 0.25H). $^{13}C\{^1H\}$-APT NMR (75 MHz, DMSO-d_6) δ 13.5 (1C), 13.6 (1C), 57.8 (1C), 60.5 (1C), 61.9 (1C), 104.2 (1C), 120.6 (1C), 124.3 (q, J = 271.0 Hz, 1C), 125.3 (1C), 127.5 (q, J = 31.5 Hz, 1C), 127.9 (2C), 128.5 (2C), 128.6 (2C), 131.0 (1C), 132.6 (2C), 143.1 (1C), 150.3 (1C), 151.5 (1C), 151.8 (1C), 161.7 (1C), 163.9 (1C), 166.6 (1C). IR (neat) (cm^{-1}) 3685, 3663, 3410, 3333, 3240, 2987, 2901, 2180, 1932, 1726, 1709, 1680, 1651, 1581, 1503, 1473, 1449, 1440, 1406, 1394, 1382, 1326, 1249, 1230, 1164, 1106, 1057, 1027, 1017, 892, 863, 842, 721, 694. HRMS (ESI+) calculated for $C_{26}H_{23}F_3N_4NaO_5$ 551.1513; found 551.1513 $[M + Na]^+$.

*2.2.14. Diethyl 6-amino-4-(4-chlorophenyl)-5-cyano-1-(2-phenylacetamido)-1,4-dihydropyridine-2,3-dicarboxylate (**7cg**)*

Following the general procedure, compound **7cg** was obtained as a pale-brown solid in 45 % yield (114.5 mg). ^1H NMR (400 MHz, DMSO-d_6) δ 0.76–1.32 (m, 6H), 3.41–3.68 (m, 2H), 3.72–4.14 (m, 4H), 4.32 (s, 0.75H), 4.46 (s, 0.25H), 6.33–6.53 (m, 2H), 7.11–7.52 (m, 9H Ar), 10.85 (s, 0.7H), 10.92 (s, 0.3H). $^{13}C\{^1H\}$-APT NMR (75 MHz, DMSO-d_6) δ 13.5 (1C), 13.6 (1C), 38.7 (1C), 61.9 (1C), 62.5 (1C), 63.8 (1C), 104.1 (1C), 120.7 (1C), 128.2 (1C), 128.3 (1C), 128.5 (1C), 128.7 (1C), 129.0 (1C), 129.5 (1C), 129.6 (1C), 130.3 (1C), 133.7 (1C), 134.7 (1C), 142.6 (1C), 144.8 (1C), 147.6 (1C), 151.1 (1C), 159.1 (1C), 164.0 (1C), 168.9 (1C), 170.8 (1C). IR (neat) (cm^{-1}) 3685, 3662, 3429, 3345, 3296, 3196, 2987, 2901, 2184, 1933, 1719, 1709, 1652, 1630, 1589, 1485, 1453, 1432, 1407, 1394, 1374, 1342, 1302, 1260, 1242, 1222, 1106, 1075, 1066, 1056, 1028, 1011, 892, 866, 835, 728, 698. HRMS (ESI+) calculated for $C_{26}H_{25}ClN_4NaO_5$ 531.1406; found 531.1406 $[M + Na]^+$.

*2.2.15. Diethyl 6-amino-5-cyano-1-(2-phenylacetamido)-4-(4-(trifluoromethyl)phenyl)-1,4-dihydropyridine-2,3-dicarboxylate (**7ck**)*

Following the general procedure, compound **7ck** was obtained as a yellow solid in 70 % yield (189.9 mg). ^1H NMR (400 MHz, DMSO-d_6) δ 0.99–1.23 (m, 6H), 3.46–3.69 (m, 2H), 3.81–4.11 (m, 4H), 4.51 (s, 0.7H), 4.57 (s, 0.3H), 6.41–6.60 (m, 2H), 7.19–7.41 (m, 5H Ar), 7.57–7.78 (m, 4H Ar), 10.88 (s, 0.7H), 10.95 (s, 0.3H). $^{13}C\{^1H\}$-APT NMR (100 MHz, DMSO-d_6) δ 13.5 (1C), 13.7 (1C), 39.2 (1C), 57.5 (1C), 60.5 (1C), 61.9 (1C), 103.9 (1C), 120.6 (1C), 125.2 (1C), 126.5 (q, J = 270.5 Hz, 1C), 126.7 (2C), 127.5 (q, J = 31.8 Hz, 1C), 128.3 (2C), 128.4 (2C), 129.5 (2C), 134.4 (1C), 142.9 (1C), 150.2 (1C), 151.2 (1C), 161.5 (1C), 163.8 (1C), 170.8 (2C). IR (neat) (cm^{-1}) 3311, 2984, 2188, 1711, 1657, 1581, 1423, 1371, 1323, 1221, 1164, 1109, 1066, 1017, 847, 730, 697. HRMS (ESI+) calculated for $C_{27}H_{25}F_3N_4NaO_5$ 565.1670; found 565.1669 $[M + Na]^+$.

*2.2.16. Diethyl 6-amino-4-(4-chlorophenyl)-5-cyano-1-octanamido-1,4-dihydropyridine-2,3-dicarboxylate (**7dg**)*

Following the general procedure, compound **7dg** was obtained as a white solid in 45 % yield (116.3 mg). ^1H NMR (300 MHz, DMSO-d_6) δ 0.74–1.60 (m, 19H), 1.98–2.33 (m, 2H), 3.84–4.05 (m, 2H), 4.09–4.27 (m, 2H), 4.33 (s, 0.75H), 4.48 (s, 0.25H), 6.35 (s, 2H), 7.20 (d, J = 7.2 Hz, 0.5H Ar), 7.30–7.60 (m, 3.5H Ar), 10.54 (s, 0.75H), 10.62 (s, 0.25H). $^{13}C\{^1H\}$-APT NMR (75 MHz, DMSO-d_6) δ 13.6 (1C), 13.7 (1C), 14.0 (1C), 22.1 (1C), 24.7 (1C), 28.5 (1C), 28.6 (1C), 31.2 (1C), 32.8 (1C), 38.7 (1C), 60.5 (1C), 61.9 (1C), 104.0 (1C), 120.8 (1C), 128.2 (1C), 128.9 (1C), 129.7 (1C), 131.5 (1C), 132.2 (1C), 142.7 (1C), 144.9 (1C), 151.2 (1C), 160.2 (1C), 161.7 (1C), 164.0 (1C), 172.8 (1C). IR (neat) (cm^{-1}) 3685, 3662, 3437, 3328, 3206, 2987, 2901, 2192, 1933, 1736, 1709, 1694, 1662, 1636, 1586, 1489, 1468, 1436, 1408, 1393, 1376, 1350, 1324, 1301, 1257, 1242, 1222, 1172, 1100, 1075, 1066, 1056, 1027, 988, 892, 860, 839, 761, 646. HRMS (ESI+) calculated for $C_{26}H_{33}ClN_4NaO_5$ 539.2032; found 539.2032 $[M + Na]^+$.

*2.2.17. Diethyl 6-amino-5-cyano-1-octanamido-4-(4-(trifluoromethyl)phenyl)-1,4-dihydropyridine-2,3-dicarboxylate (**7dk**)*

Following the general procedure, compound **7dk** was obtained as a yellow solid in 96 % yield (263.9 mg). ^1H NMR (300 MHz, DMSO-d_6) δ 0.93–1.58 (m, 19H), 2.00–2.39 (m,

2H), 3.89–3.99 (m, 2H), 4.09–4.25 (m, 2H), 4.42 (s, 0.75H), 4.58 (s, 0.25H), 6.42 (br s, 2H), 7.32–7.78 (m, 4H Ar), 10.57 (s, 0.75H), 10.65 (s, 0.25H). $^{13}C\{^{1}H\}$-APT NMR (75 MHz, DMSO-d_6) δ 13.6 (1C), 13.7 (1C), 14.0 (1C), 22.1 (1C), 24.3 (1C), 28.5 (1C), 31.1 (1C), 32.8 (1C), 39.2 (1C), 57.5 (1C), 60.6 (1C), 62.0 (1C), 103.7 (1C), 120.7 (1C), 124.4 (q, J = 276.7 Hz, 1C), 125.2 (1C), 125.6 (1C), 127.5 (q, J = 32.5 Hz, 1C), 127.9 (1C), 128.5 (1C), 143.1 (1C), 150.4 (1C), 151.3 (1C), 161.7 (1C), 163.9 (1C), 172.8 (2C). IR (neat) (cm^{-1}) 3685, 3662, 3440, 3333, 3207, 2987, 2901, 2192, 1924, 1734, 1707, 1663, 1637, 1583, 1467, 1434, 1407, 1393, 1374, 1348, 1322, 1300, 1255, 1222, 1164, 1103, 1066, 1027, 1019, 988, 892, 864, 846, 772, 686. HRMS (ESI+) calculated for $C_{27}H_{33}F_3N_4NaO_5$ 573.2295; found 573.2315 $[M + Na]^+$.

2.2.18. Diethyl 6-amino-4-(4-chlorophenyl)-5-cyano-1-(4-nitrobenzamido)-1,4-dihydropyridine-2,3-dicarboxylate (7eg)

Following the general procedure, compound **7eg** was obtained as a yellow solid in 77 % yield (207.9 mg). ^{1}H NMR (300 MHz, DMSO-d_6) δ 0.94–1.10 (m, 6H), 3.87–4.13 (m, 4H), 4.41 (br s, 1H), 6.55 (br s, 2H), 7.32–7.63 (m, 4H Ar), 8.02–8.19 (m, 2H Ar), 8.30–8.44 (m, 2H Ar), 11.66 (br s, 1H). $^{13}C\{^{1}H\}$-APT NMR (75 MHz, DMSO-d_6) δ 13.5 (1C), 13.7 (1C), 38.8 (1C), 45.8 (1C), 60.5 (1C), 61.9 (1C), 104.2 (1C), 120.9 (1C), 123.5 (2C), 128.3 (4C), 129.5 (2C), 131.5 (2C), 144.9 (2C), 149.6 (1C), 151.4 (1C), 161.8 (1C), 164.0 (2C). IR (neat) (cm^{-1}) 3674, 3420, 3330, 3218, 2987, 2901, 2200, 1933, 1709, 1688, 1663, 1600, 1527, 1474, 1406, 1379, 1344, 1324, 1298, 1228, 1181, 1075, 1066, 1056, 1028, 1015, 892, 869, 848, 840, 717. HRMS (ESI+) calculated for $C_{25}H_{22}ClN_5NaO_7$ 562.1100; found 562.1100 $[M + Na]^+$.

2.2.19. Diethyl 6-amino-5-cyano-1-(4-nitrobenzamido)-4-(4-(trifluoromethyl)phenyl)-1,4-dihydropyridine-2,3-dicarboxylate (7ek)

Following the general procedure, compound **7ek** was obtained as a yellow solid in 91 % yield (259.6 mg). ^{1}H NMR (400 MHz, DMSO-d_6) δ 0.92–1.08 (m, 6H), 3.84–4.18 (m, 4H), 4.50 (s, 0.75H), 4.61 (s, 0.25H), 6.66 (s, 1.5H), 6.70 (s, 0.5H), 7.35–7.49 (m, 0.5H Ar), 7.67–7.84 (m, 3.5H Ar), 8.00–8.20 (m, 2H Ar), 8.29–8.43 (m, 2H Ar), 11.70 (s, 0.7H), 11.74 (s, 0.3H). $^{13}C\{^{1}H\}$-APT NMR (75 MHz, DMSO-d_6) δ 13.5 (1C), 13.6 (1C), 39.2 (1C), 60.6 (1C), 62.0 (1C), 104.4 (1C), 120.6 (1C), 121.0 (1C), 123.6 (2C), 124.3 (q, J = 273.0 Hz, 1C), 125.3 (2C), 127.6 (q, J = 34.5 Hz, 1C), 128.5 (2C), 129.5 (2C), 136.7 (1C), 142.3 (1C), 149.4 (1C), 150.2 (1C), 151.3 (1C), 161.7 (1C), 163.4 (1C), 165.3 (1C). IR (neat) (cm^{-1}) 3685, 3662, 3412, 3327, 3243, 3209, 2988, 2901, 2191, 1933, 1737, 1719, 1683, 1658, 1607, 1579, 1527, 1488, 1467, 1440, 1406, 1394, 1371, 1322, 1303, 1266, 1250, 1220, 1173, 1100, 1076, 1065, 1027, 1016, 989, 891, 868, 848, 835, 792, 709, 601. HRMS (ESI+) calculated for $C_{26}H_{22}F_3N_5NaO_7$ 596.1364; found 596.1348 $[M + Na]^+$.

2.2.20. Diethyl 6-amino-1-(4-chlorobenzamido)-4-(4-chlorophenyl)-5-cyano-1,4-dihydropyridine-2,3-dicarboxylate (7fg)

Following the general procedure, compound **7fg** was obtained as a white solid in 44 % yield (116.5 mg). ^{1}H NMR (400 MHz, DMSO-d_6) δ 0.93–1.09 (m, 6H), 3.87–4.16 (m, 4H), 4.39 (s, 0.75H), 4.50 (s, 0.25H), 6.51 (s, 1.5H), 6.56 (br s, 0.5H), 7.24 (d, J = 7.2 Hz, 0.5H Ar), 7.35–7.47 (m, 2H Ar), 7.51–7.68 (m, 3.5H Ar), 7.85 (d, J = 7.9 Hz, 0.5H Ar), 7.91 (d, J = 7.9 Hz, 1.5H Ar), 11.37 (s, 0.75H), 11.44 (s, 0.25H). $^{13}C\{^{1}H\}$-APT NMR (75 MHz, DMSO-d_6) δ 13.5 (1C), 13.7 (1C), 38.7 (1C), 60.5 (1C), 61.9 (1C), 104.1 (1C), 120.8 (1C), 128.3 (2C), 128.6 (2C), 129.7 (2C), 129.9 (2C), 131.5 (1C), 137.5 (1C). 142.6 (1C), 144.8 (1C), 151.3 (1C), 151.7 (1C), 161.80 (1C), 164.0 (1C), 165.0 (1C), 165.7 (1C). IR (neat) (cm^{-1}) 3685, 3674, 3452, 3318, 3234, 3199, 2987, 2873, 2901, 2186, 1916, 1726, 1703, 1660, 1635, 1583, 1493, 1474, 1453, 1434, 1406, 1394, 1371, 1348, 1312, 1266, 1242, 1219, 1181, 1076, 1066, 1057, 1027, 1014, 892, 861, 837, 760, 667. HRMS (ESI+) calculated for $C_{25}H_{22}Cl_2N_4NaO_5$ 551.0859; found 551.0859 $[M + Na]^+$.

2.2.21. Diethyl 6-amino-1-(4-chlorobenzamido)-5-cyano-4-(4-(trifluoromethyl)phenyl)-1,4-dihydropyridine-2,3-dicarboxylate (7fk)

Following the general procedure, compound **7fk** was obtained as a yellow solid in 92 % yield (258.9 mg). ^{1}H NMR (300 MHz, DMSO-d_6) δ 0.94–1.16 (m, 6H), 3.83–4.25 (m, 4H), 4.55 (s, 1H), 6.57 (s, 2H), 7.43–8.01 (m, 8H Ar), 11.40 (br s, 1H). $^{13}C\{^{1}H\}$-APT NMR (75 MHz, DMSO-d_6) δ 13.5 (1C), 13.6 (1C), 39.0 (1C), 60.5 (1C), 61.9 (1C), 104.0 (1C), 120.6 (1C), 124.3 (q, J = 271.3 Hz, 1C), 125.3 (2C), 127.5 (q, J = 33.2 Hz, 1C), 128.5 (4C), 129.8 (2C), 130.1 (1C), 137.3 (1C), 149.8 (2C), 151.5 (2C), 161.7 (1C), 163.9 (2C). IR (neat) (cm^{-1}) 3685, 3674, 3466, 3329, 3206, 2987, 2901, 2186, 1933, 1706, 1655, 1617, 1581, 1505, 1476, 1406, 1394, 1380, 1323, 1249, 1241, 1226, 1162, 1066, 1027, 1015, 892, 865, 844, 757. HRMS (ESI+) calculated for $C_{26}H_{22}ClF_3N_4NaO_5$ 585.1123; found 585.1116 $[M + Na]^+$.

2.2.22. Diethyl 6-amino-4-(4-chlorophenyl)-5-cyano-1-(4-methoxybenzamido)-1,4-dihydropyridine-2,3-dicarboxylate (7gg)

Following the general procedure, compound **7gg** was obtained as a pale-brown solid in 57 % yield (149.6 mg). ^{1}H NMR (300 MHz, DMSO-d_6) δ 0.94–1.13 (m, 6H), 3.84 (s, 3H), 3.90–4.19 (m, 4H), 4.39 (s, 0.75H), 4.51 (s, 0.25H), 6.40 (s, 1.5H), 6.45 (s, 0.5H), 6.99–7.11 (m, 2H Ar), 7.21–7.29 (m, 0.5H Ar), 7.36–7.48 (m, 2H Ar), 7.54–7.63 (m, 1.5H Ar), 7.78–7.96 (m, 2H Ar), 11.08 (s, 0.75H), 11.19 (s, 0.25H). $^{13}C\{^{1}H\}$-APT NMR (75 MHz, DMSO-d_6) δ 13.5 (1C), 13.7 (1C), 39.0 (1C), 55.5 (1C), 60.5 (1C), 61.8 (1C), 104.2 (1C), 113.6 (1C), 113.7 (1C), 120.8 (1C), 123.2 (1C), 128.2 (1C), 128.5 (1C), 129.0 (1C), 129.9 (1C), 130.0 (1C), 131.5 (1C), 142.9 (1C), 144.9 (1C), 151.4 (1C), 151.8 (1C), 161.8 (1C), 162.6 (1C), 164.0 (1C), 165.3 (1C), 165.9 (1C). IR (neat) (cm^{-1}) 3674, 3464, 3308, 3222, 3191, 2987, 2901, 2185, 1932, 1727, 1703, 1657, 1634, 1606, 1579, 1477, 1436, 1406, 1394, 1374, 1309, 1262, 1246, 1177, 1103, 1076, 1066, 1056, 1028, 892, 868, 835, 766, 567. HRMS (ESI+) calculated for $C_{26}H_{25}ClN_4NaO_6$ 547.1355; found 547.1355 $[M + Na]^+$.

2.2.23. Diethyl 6-amino-5-cyano-1-(4-methoxybenzamido)-4-(4-(trifluoromethyl)phenyl)-1,4-dihydropyridine-2,3-dicarboxylate (7gk)

Following the general procedure, compound **7gk** was obtained as a brown solid in 51 % yield (142.4 mg). ^{1}H NMR (300 MHz, DMSO-d_6) δ 0.96–1.15 (m, 6H), 3.86 (s, 3H),

3.98 (q, J = 7.1 Hz, 2H), 4.03–4.23 (m, 2H), 4.52 (s, 0.75H), 4.65 (br s, 0.25H), 6.38–6.54 (m, 2H), 7.00–7.15 (m, 2H Ar), 7.42–7.56 (m, 0.5H Ar), 7.70–8.03 (m, 5.5H Ar), 11.11 (br s, 0.75H), 11.22 (br s, 0.25H). $^{13}C\{^{1}H\}$-APT NMR (75 MHz, DMSO-d_6) δ 13.5 (1C), 13.6 (1C), 30.7 (1C), 55.5 (1C), 60.5 (1C), 61.8 (1C), 104.0 (1C), 113.7 (2C), 120.6 (1C), 123.2 (1C), 124.3 (q, J = 273.2 Hz, 1C), 125.2 (2C), 127.5 (q, J = 32.0 Hz, 1C), 128.6 (2C), 129.9 (2C), 143.2 (1C), 150.3 (1C), 151.5 (1C), 161.7 (1C), 162.6 (1C), 163.9 (1C), 166.0 (2C). IR (neat) (cm^{-1}) 3685, 3671, 3477, 3316, 3206, 2987, 2901, 2186, 1932, 1706, 1655, 1605, 1578, 1465, 1406, 1394, 1381, 1323, 1250, 1241, 1228, 1173, 1105, 1066, 1027, 892, 866, 873, 767, 559. HRMS (ESI+) calculated for $C_{27}H_{25}F_3N_4NaO_6$ 581.1618; found 581.1606 $[M + Na]^+$.

2.3. Cell culture

HeLa (human cervical carcinoma), A549 (human lung carcinoma) and MIA PaCa-2 (human pancreatic carcinoma, kindly provided by Dr. Guillermo Velasco, UCM, Spain) cell lines were cultured in high glucose DMEM (Dulbecco's Modified Eagle's Medium) supplemented with 5 % fetal bovine serum (FBS). Jurkat, clone E6.1 (human acute T cell leukemia) cell line (from ATCC, USA) was routinely cultured in RPMI 1640 medium supplemented with 10 % fetal bovine serum (FBS). All media incorporated L-glutamine in the form of GlutaMAX and penicillin/streptomycin. Cultures were maintained at 37 °C in a humidified atmosphere of 95 % air/5 % CO_2.

2.4. Cytotoxicity assay

The MTT assay was used to determine cell viability as an indicator of cell sensitivity to the compounds. Exponentially growing cells were seeded at a density of approximately 10^4 cells per well (HeLa, A549 and MIA PaCa-2) or $1.5x10^5$ cells per well (Jurkat) in 96-well flat-bottom microplates (100 µL/well) and allowed to adhere for 24 h before addition of the compounds. The compounds were dissolved in DMSO and added to the cells at concentrations from 1 to 100 µM in quadruplicate. They were then left to incubate for 24 h or 72 h at 37 °C. After this time, 10 µL of MTT (5 mg/mL) were added to each well and incubated again for 2 h at 37 °C. Finally, the culture medium was removed (plates were centrifuged beforehand for 20 min at 2500 rpm in the case of Jurkat cells) and 100 µL of DMSO per well was added to dissolve the formazan crystals. Optical density was measured at 550 nm using a 96-well multiscanner autoreader (ELISA). The IC_{50} was calculated by non-linear regression using *Origin Pro* software. Each compound was assayed a minimum of 3 times independently.

2.5. Cell death analysis

Phosphatidylserine exposure (PS) on the cell surface and cell membrane permeabilization were measured to detect apoptotic and necrotic cell death in Jurkat and MIA PaCa-2 cell lines. For leukemic cells, $1.5x10^5$ cells/well were seeded in complete RPMI 1640 medium in flat-bottom, 48-well plates (500 µL/well) and treated with compounds **7dk** and **7dg** for 24 h and 72 h, respectively, at concentrations of 5, 10 and 20 µM in duplicate. On the other hand, $5x10^4$ cell/well of pancreatic cells were seeded in complete DMEM medium in flat-bottom, 24-well plates (500 µL/well), allowed to attach to the substrate for 24 h and treated for 24 h with compounds **7dk** and **7dg** at concentrations ranging from 5 to 45 µM also in duplicate. To assess the role of caspases in the death mechanism and the involvement of necroptosis, cells were preincubated for 1 h with the pan-caspase inhibitor Z-VAD-fmk (30 µM) or the necroptosis inhibitor Necrostatin-1 (MedChemExpress, USA) prior to the addition of the compounds. After treatment, Jurkat cells were directly labeled but MIA PaCa-2 cells were previously trypsinized. In any case, cells were resuspended in 100 µL of a mixture of Annexin-binding buffer (ABB; 140 mM NaCl, 2.5 mM $CaCl_2$, 10 mM HEPES/NaOH pH 7.4), DY634-conjugated Annexin-V and 7-amino-actinomycin D (7-AAD) and incubated at room temperature in the dark for 15 min. Finally, cells were diluted to 300 µL with PBS and a total of 10,000 cells were acquired on a FACSCalibur™ flow cytometer (BD, Biosciences, USA). Cell death was analyzed using CellQuest Pro (BD Biosciences), FlowJo 7.6.1 (Becton Dickinson (BD), USA) and GraphPad Prism 8.0.1. (GraphPad Software, USA) software.

2.6. Mitochondrial transmembrane potential analysis

The integrity of the mitochondrial outer membrane was assessed by measuring the disruption of mitochondrial transmembrane potential. To this end, $1.5x10^5$ Jurkat cells and 10^5 MIA PaCa-2 cells were seeded in the appropriate complete medium in flat-bottom, 48-well plates (500 µL/well) and 12-well plates (1 mL/well), respectively. Jurkat cells were immediately exposed to compounds **7dk** and **7dg** for 24 and 72 h, respectively, at concentrations of 5, 10 and 20 µM in duplicate. For their part, MIA PaCa-2 cells were treated once they had attached to the bottom with compounds **7dk** and **7dg** for 24 h at concentrations ranging from 5 to 45 µM also in duplicate and they were trypsinized before staining. Subsequently, cells were resuspended in 500 µL of a mixture of complete medium and 60 nM of the tetramethylrhodamine ethyl ester (TMRE) probe and incubated at 37 °C in the dark for 20 min. Finally, a total of 10000 events were acquired on a FACSCalibur™ flow cytometer and data were analyzed using the aforementioned software.

2.7. In vivo assays

All experiments followed the PI87/20 research procedures approved by the ethics committee for animal experiments of the University of Zaragoza. Animal care and use were carried out in accordance with the Spanish policy for animal protection RD53/2013 and the European Union directive 2010/63 for the protection of animals used for experimental and other scientific purposes. Adult male (9–13 weeks) RjOrl:SWISS mice from Janvier Laboratories were used. Up to a maximum of 5 specimens were kept in 30 x 20 x 15 cm boxes, with access to water and food *ad libitum*. The room temperature was maintained at 23 ± 1 °C with a 12 h light cycle (starting at 7:00 a.m.). Drugs were administered orally (PO) or intraperitoneally to conscious mice with a standard volume of 10 mL/kg body weight. Test compounds were administered as a suspension in physiological saline (5 % DMSO). Animals were monitored individually at least once during the first 30 min after injection,

periodically during the first 24 h (with special attention to the first 4 h) and daily thereafter for a total of 14 days.

The health status of the animals was monitored using a modified scale based on the proposal by Morton and Griffiths. General appearance (0–3), weight (0–2), spontaneous behavior (0–3), and provoked behavior (0–3) were scored (Table S6).

3. Results and discussion

3.1. Synthesis of *N*-benzamido-1,4-dihydropyridines

We started the study by synthesizing a battery of *N*-benzamido-1,4-dihydropyridines **7** following our own experience to obtain highly functionalized 1,4-dihydropyridines (Auria-Luna et al., 2015, 2017, 2018, 2020). From previous asymmetric synthesis of this family of compounds (Auria-Luna et al., 2015, 2017), we realized about the importance of bearing a base in the chiral catalyst structure. Therefore, to develop this work we tested simple organic bases (DABCO, Et_3N and pyridine). From a preliminary exploration, Et_3N was selected as the most accessible and efficient catalyst base to expand this procedure. Moreover, we simply studied the procedure at room temperature, in order to avoid consuming energy and since we obtained really good yields in the model reaction. Therefore, 1,4-DHPs **7aa**, **7ai**, **7ba-bj** were catalytically synthesized following a simple and straightforward protocol and giving rise to the final products with moderate to excellent yields (from 19 to 96 %) (Scheme 1 and Fig. 2).

Based on our previously reported mechanisms for the asymmetric version of this synthesis (Auria-Luna et al., 2015, 2017), we herein propose a reasonable mechanism depicted in Scheme 2.

The synthesized hydrazones **3** are in equilibrium with their enamine form in the presence of the organic base (**A**). Then, the generated enamine would attack to the malononitrile **6** via a Michael addition (**B**). Afterward, the intermediate hydrazone formed in the medium (**C**), in equilibrium with its enehydrazide form (enamine) (**D**), would attack to a nitrile group via an intramolecular nucleophilic addition of the NH (**D**). This addition would close the piperidine ring in the intermediate (**E**). Final 1-benzamido-1,4-dihydropyridines **7** would be generated after a subsequent tautomerization of the intermediate (**E**) (Scheme 2).

This group of compounds has been initially chosen as a characteristic family bearing different steric and electronic properties in the aromatic ring of the starting malononitrile **6**. From the different possibilities of functionalization on the 1,4-DHP core, the aryl group at the C4 position has been first selected as one of the main structural variables. This variety of 1,4-DHP derivatives could exemplify a preliminary representative structure–activity relationship.

3.2. Cytotoxicity study

With this family of compounds in hand, we carried out the first biological experiments. Moreover, to clarify if the substitution in the ester could also exhibit a pivotal role in the biological activity, we also synthesized two structures with a methyl group instead of an ethyl group (**7aa** and **7ai**).

First, a cytotoxicity study was carried out with all compounds against four different cancer cell lines: HeLa (human cervical carcinoma), Jurkat (leukemia), A549 (human lung cancer) and MIA PaCa-2 (pancreatic cancer). The measurement of the cytotoxic activity was performed using the MTT assay (van Meerloo et al., 2011) and the results are disclosed in Fig. 3.

Based on the results obtained for this first block of compounds (Fig. 3), different conclusions can be stated. If a first comparison is made between compounds **7aa** and **7ba** or **7ai** and **7bi**, whose only difference appears in the dicarboxylate residue, it is found that the toxicity in all tumor lines studied is higher for compound **7ba**, with the ethyl ester instead of the methyl one **7aa**. However, after the introduction of an electron withdrawing substituent in the ring of benzylidenemalononitrile (**7ai** and **7bi**), the trend seems to be reverse. Nevertheless, we could not assume a general behavior, since only two examples with this variation have been studied.

Furthermore, it seems that there is certain selectivity towards the different cancer cell lines, with scarce or no cytotoxicity in the case of HeLa and promising results with Jurkat cells, in general for all tested compounds.

From these preliminary outcomes, it is also possible to predict some structure–activity relationships. Based on the type of structure or the possibility of charge delocalization derived from the position of the electro-withdrawing group in the aromatic ring, a marked influence on the results can be observed. Hence, if compounds **7bd** and **7bf** are compared, isomers that differ in the position of the nitro group on the aromatic ring at the benzylidenemalononitrile **6**, 50 % of cell viability was not reached in the assay conditions for HeLa and A549 cell lines

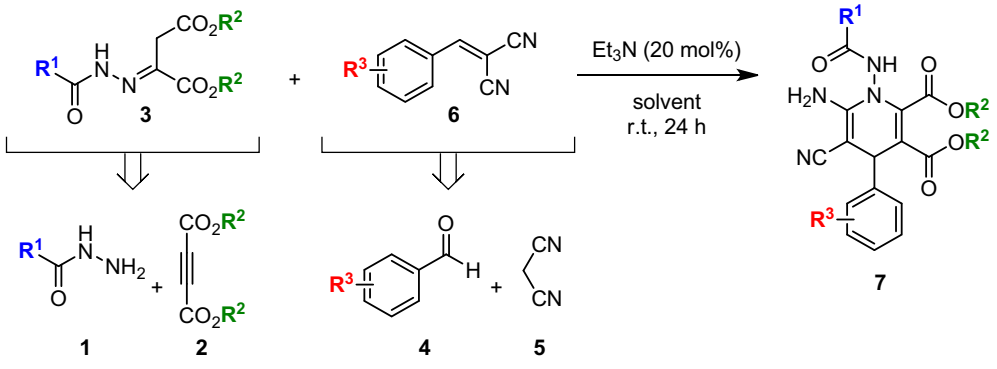

Scheme 1 Synthesis of 1-benzamido-1,4-dihydropyridines **7**.

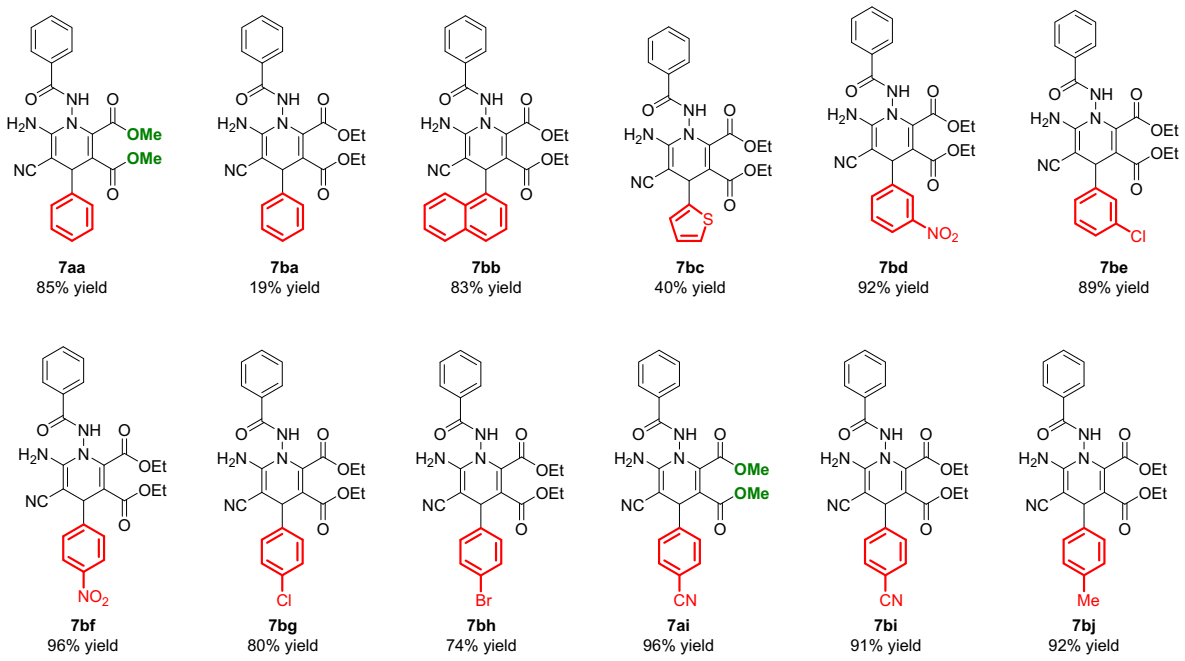

Fig. 2 Structures of 1-benzamido-1,4-dihydropyridines **7aa**, **7ai**, **7ba-bj** (block 1).

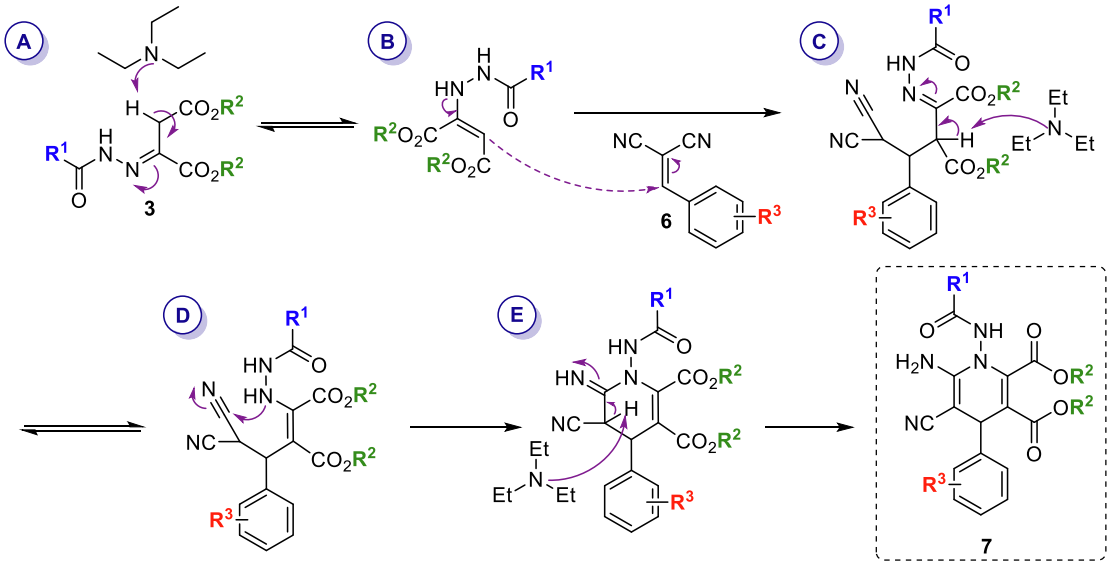

Scheme 2 Plausible reaction mechanism.

for compound **7bd**, with the substituent in *meta*-position. In contrast, compound **7bf**, with the same substituent in *para*, presents higher IC_{50} values for both lines and lower in the other two cancer cell lines.

If a comparison is made between the different electron-donor / acceptor properties of the selected benzylidene-malononitrile **6**, it can also be concluded that those compounds with electro-withdrawing substituents such as **7bd-bh** mostly present better results in the lines studied than species **7bj**, with a methyl moiety in the aromatic ring (4-MeC_6H_4).

In the same way, it is remarkable that analogous compounds **7bg** (4-ClC_6H_4) and **7bh** (4-BrC_6H_4), both with a halogen in *para*, present clear differences in terms of selectivity for all lines studied. Therefore, while the chloro derivative **7bg** shows moderate to good results in all of them, the bromo one **7bh** does not reach levels of 50 % inhibition in HeLa although it presents better results in Jurkat or A549.

Considering this structure–activity relationship, it is possible to conclude that the cytotoxicity results are dependent on the malononitrile precursors, showing the best IC_{50} values for derivatives with electro-withdrawing substituents on them. Specifically, compound **7bg** (4-ClC_6H_4) provided, in general, the best cytotoxicity values for the four tumor lines tested.

Once this trend was known and assessed, a second series of compounds was synthesized, in this case, with the malononitrile derivatives as fixed precursors and making the respective variations in the hydrazone residue **3**.

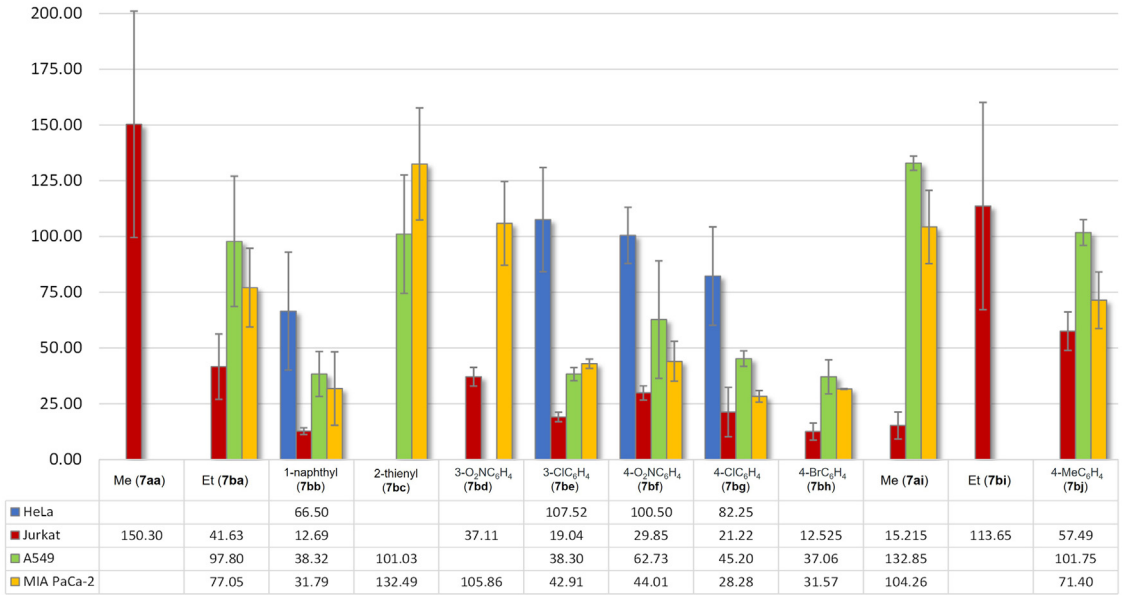

	Me (**7aa**)	Et (**7ba**)	1-naphthyl (**7bb**)	2-thienyl (**7bc**)	3-$O_2NC_6H_4$ (**7bd**)	3-ClC_6H_4 (**7be**)	4-$O_2NC_6H_4$ (**7bf**)	4-ClC_6H_4 (**7bg**)	4-BrC_6H_4 (**7bh**)	Me (**7ai**)	Et (**7bi**)	4-MeC_6H_4 (**7bj**)
HeLa			66.50			107.52	100.50	82.25				
Jurkat	150.30	41.63	12.69		37.11	19.04	29.85	21.22	12.525	15.215	113.65	57.49
A549		97.80	38.32	101.03		38.30	62.73	45.20	37.06	132.85		101.75
MIA PaCa-2		77.05	31.79	132.49	105.86	42.91	44.01	28.28	31.57	104.26		71.40

Fig. 3 IC_{50} values (μM) for 1,4-DHPs **7aa**, **7ai**, **7ba-bj** after 24 h. Error bars represent the standard deviation for 3 independent experiments. Empty boxes show those experiments in which 50 % of cell viability was not reached in the assay conditions. The complete data with error values can be found in the supporting information, Table S1.

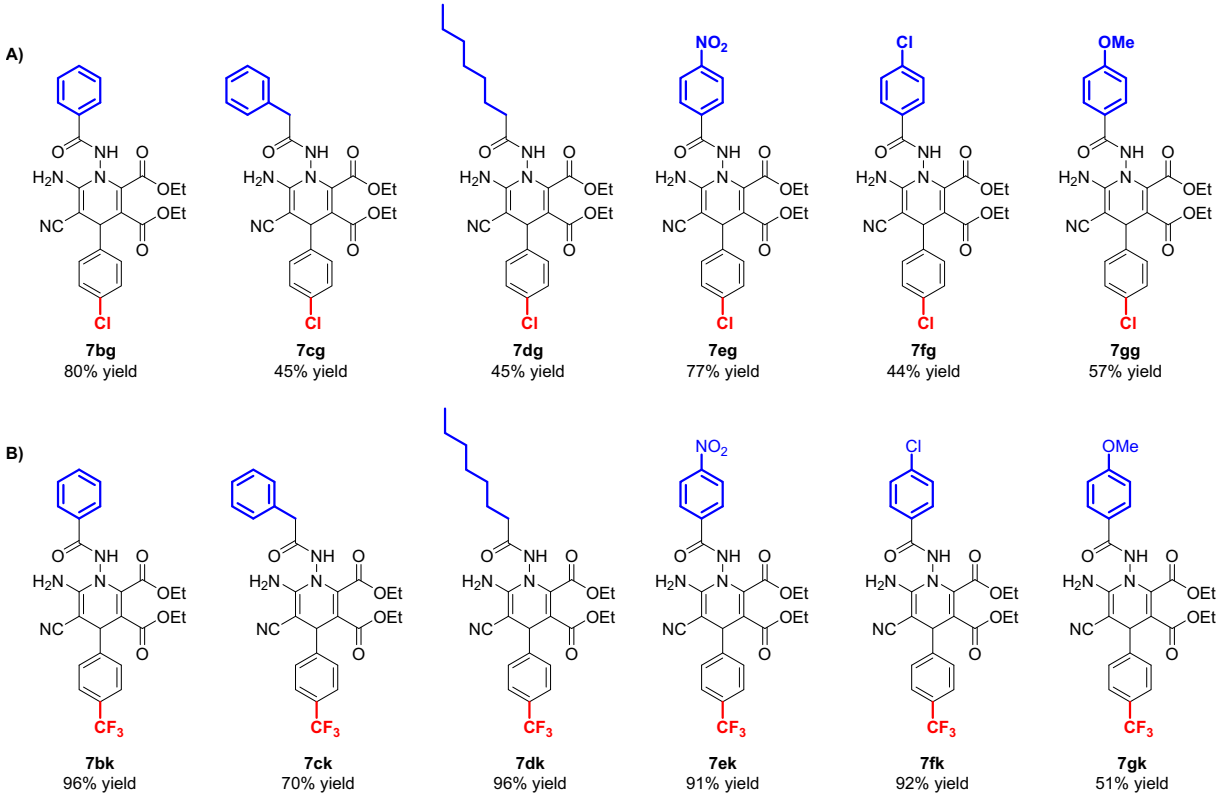

Fig. 4 Structures of 1-benzamido-1,4-dihydropyridines **7bg-gg** (block 2A) and **7bk-gk** (block 2B).

In this sense, with the main goal of developing more structural diversity and giving rise to anticancer drugs with better activities, we further synthesized five additional derivatives bearing the *para*-Cl group **6g** fixed in the aromatic ring (Fig. 4, block 2A). Additionally, evaluating the electronic properties of the compounds with the presence of a CF_3 group

and working under the hypothesis that this moiety could increase the bioavailability of the resulting structures in the cellular environment (Shah and Westwell, 2007; Gillis et al., 2015) a 4-$F_3CC_6H_4$ group (**6k**) was selected as a fixed precursor for the synthesis of 6 new derivatives (Fig. 4, block 2B).

Then, using the same general synthetic protocol disclosed in Scheme 1, a total of 12 derivatives were obtained with moderate to excellent yields (from 44 to 96 %), being the first example in the literature of this kind of interesting derivatives. Hence, with them in hand, we proceed with the biological tests, firstly with block 2A (Fig. 5).

As can be seen in Fig. 5, variation in the hydrazone moiety of precursor **3**, in almost all cases, implies an improvement in the IC_{50} value for all lines studied in comparison with **7bg**. Only for compound **7eg**, with the 4-$O_2NC_6H_4$ substitution, the values of IC_{50} are somehow higher.

In addition, it is noticeable that the introduction of new substituents in the starting hydrazone **3** has led to a very notable increase in cytotoxicity towards the HeLa tumor line, whose values were moderately high in the derivatives of block 1 and in this case, they are better and below 40 μM in some cases. Focusing on HeLa cells, it is revealed that the electronegativity of the substituent introduced in precursor **3** is not decisive in terms of cytotoxicity. Compound **7eg** (4-$O_2NC_6H_4$) shows the worst IC_{50} value for this line (60.12 μM), while compound **7fg** (4-ClC_6H_4) bearing an electronegative substituent presents the lowest value for the same line (21.64 μM). This seems to indicate that not only the electronic characteristics of the substituent influence the activity but also the structure by itself plays a fundamental role. This low selectivity, in terms of electronic properties, is reflected again if a comparison is made between opposing groups such as 4-$O_2NC_6H_4$ of **7eg** and 4-$MeOC_6H_4$ of **7gg**. The MeO group, which is a good electron density donor, presents IC_{50} values in all cases lower than **7eg**, although higher than other derivatives with electron-withdrawing groups, such as **7fg** (4-ClC_6H_4). This same controversial situation is manifested if we focus on the two best compounds: **7fg** and **7dg**, the first of them with a *para* chlorine substitution and the second, with an alkyl chain of seven carbon atoms. In both cases, similar results and similar selectivity are observed for the different cell lines.

Additionally, and in parallel to this block 2A, the derivatives **7bk-7gk** (Fig. 4, block 2B), with a CF_3 moiety were also explored (Fig. 6).

As expected, changing the Cl group in *para* position by a substituent with greater biocompatibility resulted in a notable improvement of the IC_{50} values in all cancer cell lines (Fig. 6).

Again, the increase in selectivity towards the HeLa line is noteworthy, except for compound **7bk** which did not present any toxicity against this line. The remaining compounds exhibit activity against all cancer cell lines assayed, even reaching values of 15.52 μM in the case of **7dk** (heptyl), better than its chloro analog **7dg** (29.93 μM) at the block 2A, although the best results were obtained for Jurkat and MIA PaCa-2 cell lines. Additionally, when the study was performed with the most active structure **7dk** during 72 h instead of 24 h, for the four cell lines, better values of cytotoxicity were achieved in all cases as reported in Fig. 7.

In general, this derivatization process proved to be useful, observing a gradual increase in cytotoxicity of all new compounds tested. Furthermore, these results might be of interest due to the presence of selectivity in the behavior of the abovementioned compounds against specific cancer cell lines, which may become an attractive characteristic for new drug discovery.

3.3. Additional biological tests

To explore more precisely the activity of the best working compounds in the MTT assays (**7dk** and **7dg**), a series of additional biological tests were performed, including cytotoxicity assays,

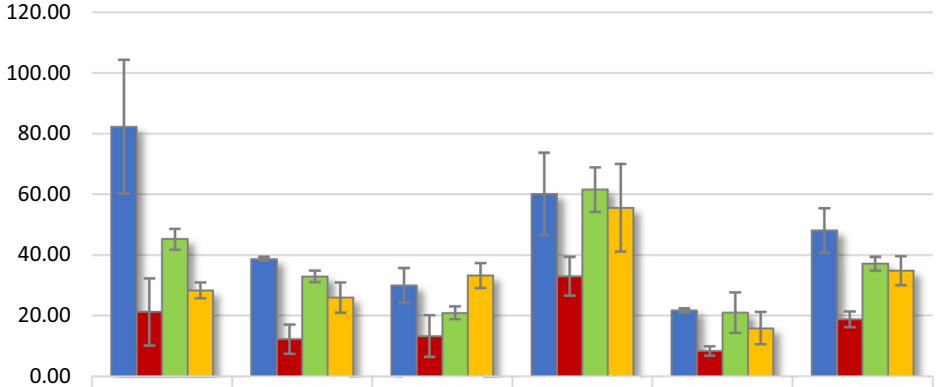

	Ph (**7bg**)	$CH_2C_6H_5$ (**7cg**)	heptyl (**7dg**)	4-$O_2NC_6H_4$ (**7eg**)	4-ClC_6H_4 (**7fg**)	4-$MeOC_6H_4$ (**7gg**)
HeLa	82.25	38.68	29.93	60.12	21.64	48.05
Jurkat	21.22	12.24	13.24	32.98	8.27	18.78
A549	45.20	32.90	20.88	61.57	20.93	37.10
MIA PaCa-2	28.28	25.96	33.20	55.55	15.85	34.80

Fig. 5 IC_{50} values (μM) for 1,4-DHPs **7bg-gg** after 24 h. Error bars represent the standard deviation for 3 independent experiments. Empty boxes show those experiments in which 50 % of cell viability was not reached in the assay conditions. The complete data with error values can be found in the supporting information, Table S2.

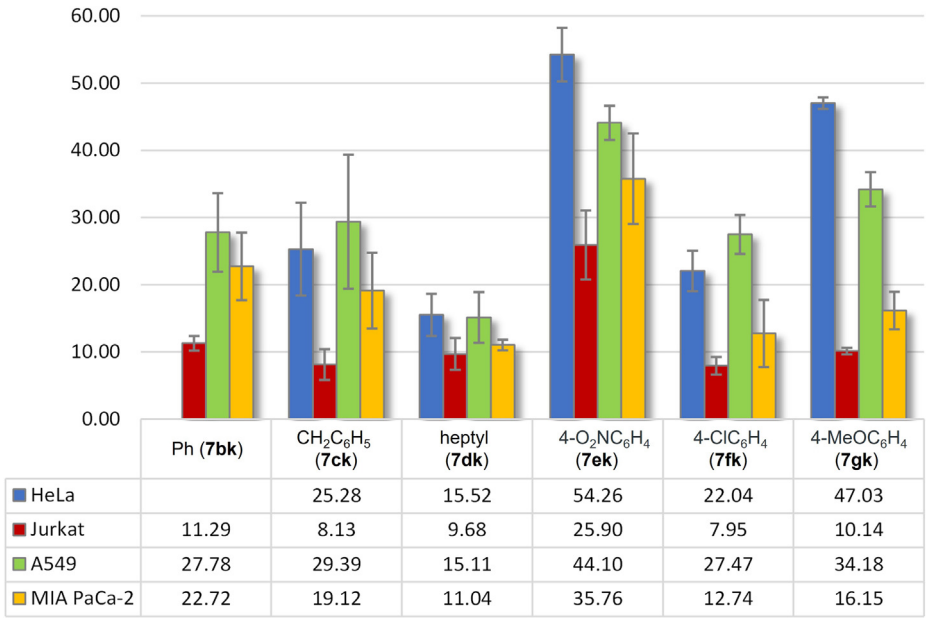

	Ph (**7bk**)	$CH_2C_6H_5$ (**7ck**)	heptyl (**7dk**)	4-$O_2NC_6H_4$ (**7ek**)	4-ClC_6H_4 (**7fk**)	4-$MeOC_6H_4$ (**7gk**)
HeLa		25.28	15.52	54.26	22.04	47.03
Jurkat	11.29	8.13	9.68	25.90	7.95	10.14
A549	27.78	29.39	15.11	44.10	27.47	34.18
MIA PaCa-2	22.72	19.12	11.04	35.76	12.74	16.15

Fig. 6 IC_{50} values (μM) for 1,4-DHPs **7bk-gk** after 24 h. Error bars represent the standard deviation for 3 independent experiments. Empty boxes show those experiments in which 50 % of cell viability was not reached in the assay conditions. The complete data with error values can be found in the supporting information, Table S3.

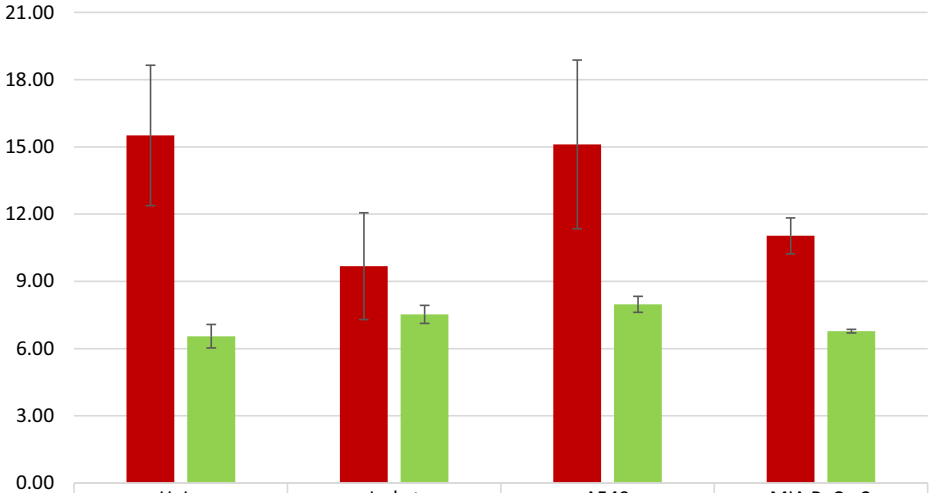

	HeLa	Jurkat	A549	MIA PaCa-2
24 h	15.52	9.68	15.11	11.04
72 h	6.55	7.53	7.98	6.78

Fig. 7 IC_{50} values (μM) for 1,4-DHP **7dk** in a comparative study for 72 h and 24 h. Error bars represent the standard deviation for 3 independent experiments. The complete data with error values can be found in the supporting information, Table S4.

cell death mechanism studies and assessment of mitochondrial transmembrane potential. Working under the same criteria, the tumor cell lines studied with these compounds were Jurkat and MIA PaCa-2, as they were the two cell lines with the lowest IC_{50} values (9.7 μM and 13.2 μM for Jurkat and 11.0 μM and 33.2 μM for MIA PaCa-2, respectively).

3.3.1. Morphological appearance

Cellular behavior and prominent morphological alterations resulting from their exposure to compounds were analyzed under an inverted microscope. While untreated cells were healthy, grew exponentially and exhibited their characteristic morphology (lymphoblast-like in the case of Jurkat cells and epithelial-like with floating rounded cells in the case of MIA PaCa-2 cells), treated ones were significantly disturbed the higher the dose, especially MIA PaCa-2 cells (Fig. 8). It should be noted that the response of each cell type to each compound is different.

Jurkat cells only changed their appearance with the highest concentration of **7dk**, with which the presence of a large num-

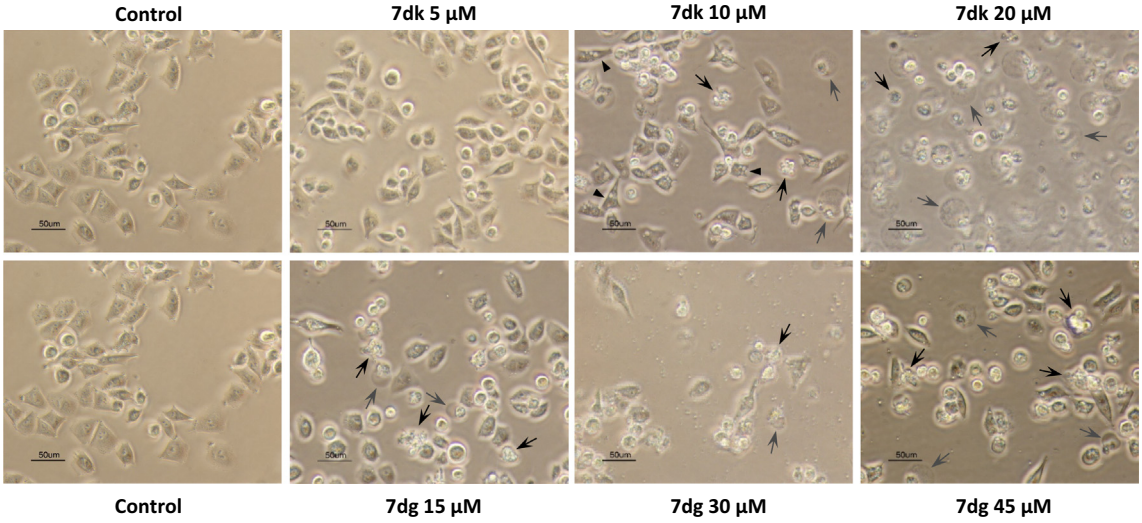

Fig. 8 Phase-contrast microscopy images of MIA PaCa-2 cells exposed to increasing concentrations of **7dk** and **7dg** for 24 h. Black and grey arrows point to examples of apoptotic and necrotic cells, respectively. Little black triangles denote cells containing cytoplasmic vacuoles.

ber of dead cells was evident after 24 h of treatment (data not shown). However, few signs of cell death were detected with **7dg** whatever the dose despite treatment being extended up to 72 h (data not shown). A different behavior was found with MIA PaCa-2 cells, which were already affected by both compounds at 24 h in different ways. The appearance they presented when treated with the lowest dose of **7dk** was similar to that of healthy cells, but when they were faced with the highest dose, the majority of the cell population exhibited a clearly apoptotic and necrotic morphology (Fig. 8). Additionally, with the intermediate concentration, it is possible to identify vacuoles of different sizes in the cytoplasm, in addition to apoptotic and necrotic cells (Fig. 8). Nevertheless, **7dg** induced apoptotic and necrotic morphology at a similar level regardless of dose and cytoplasmic vacuolization was not detected (Fig. 8).

3.3.2. Cytotoxic potential and cell death mechanism

To further explore the effect of the compounds on both cell lines, several flow-cytometry studies were carried out. Firstly, we evaluated their ability to promote cell death based on specific cell death markers, in particular phosphatidylserine (PS) exposure on the outer face of the plasma membrane to detect apoptosis and plasma membrane permeabilization to identify necrosis. The presence of PS on the cell surface is indicative of an 'early apoptotic', event that can be measured by flow cytometry thanks to Annexin-V protein conjugated with different fluorophores, while the integrity of the plasma membrane is compromised in the so-called 'late apoptosis' and can be tested with DNA intercalating agents (Stojak et al., 2013). In this case, we have used DY634-conjugated Annexin-V and the DNA-labelling dye 7-AAD.

At first glance in Fig. 9, the cytotoxic potential of the compounds is greater the higher the dose, but substantial differences in the response of both cell lines to each species are observed. Compound **7dk** displays an extraordinary cytotoxic potential at higher concentrations in both cell lines after 24 h of treatment (Fig. 9: A and C). Conversely, **7dg** is less effective for this purpose, since only a modest cytotoxic effect is observed in MIA PaCa-2 cells at 24 h at the highest doses (Fig. 9D), and in Jurkat cells, the cell death induced is scarce even at high doses and exposition times (Fig. 9B). In the latter case, it is remarkable that only 20 % death is observed at a concentration of 20 µM when the IC_{50} value resulting from the MTT assays at 24 h is close to 10 µM. This suggests that **7dg** rather exerts a cytostatic effect in Jurkat cells. According to labeling, late apoptosis (Annexin-V-DY634+/7-AAD+) is the main cell fate in both cell types with the two compounds. Moreover, while early apoptotic (Annexin-V-DY634+/7-AAD-) or necrotic (Annexin-V-DY634-/7-AAD+) Jurkat cells are barely detected with both compounds, in MIA PaCa-2 cells early apoptosis is somewhat more common, and in some cases even necrosis (Fig. 9). Therefore, these data partially support microscopy observations.

Based on these results, we decided to delve into the mechanism of death associated with the compounds, except in the case of leukemic cells treated with **7dg**, which were excluded, as they did not reach a noticeable death threshold. Specifically, we evaluated the involvement of caspases as crucial mediators of apoptosis (Sadowski-Debbing et al., 2002) and we wanted to find out if necroptosis, a novel type of necrotic-like, caspase-independent programmed cell death (Dunai et al., 2012), was unleashed. The pan-caspase inhibitor Z-VAD-fmk and the necroptosis inhibitor Necrostatin-1 (Nec-1) were used to unveil the role of caspases and the activation of necroptosis, respectively. Fig. 10 shows the poor ability of Z-VAD-fmk to prevent the cell death triggered by **7dk** in both cell lines. Nec-1 has no effect on cells treated with this compound and the combination of both inhibitors does not enhance the inhibitory effect of Z-VAD-fmk alone (Fig. 11: A and B). Intriguingly, at the concentration that large vacuolization occurs in MIA PaCa-2 cells, both inhibitors separately or in combination increase the populations of the early and late apoptotic cells (Fig. 11B), while the level of vacuolization appears to decrease slightly in these situations (Fig. 10). By contrast, neither Z-VAD nor Nec-1 and the combination of both inhibitors man-

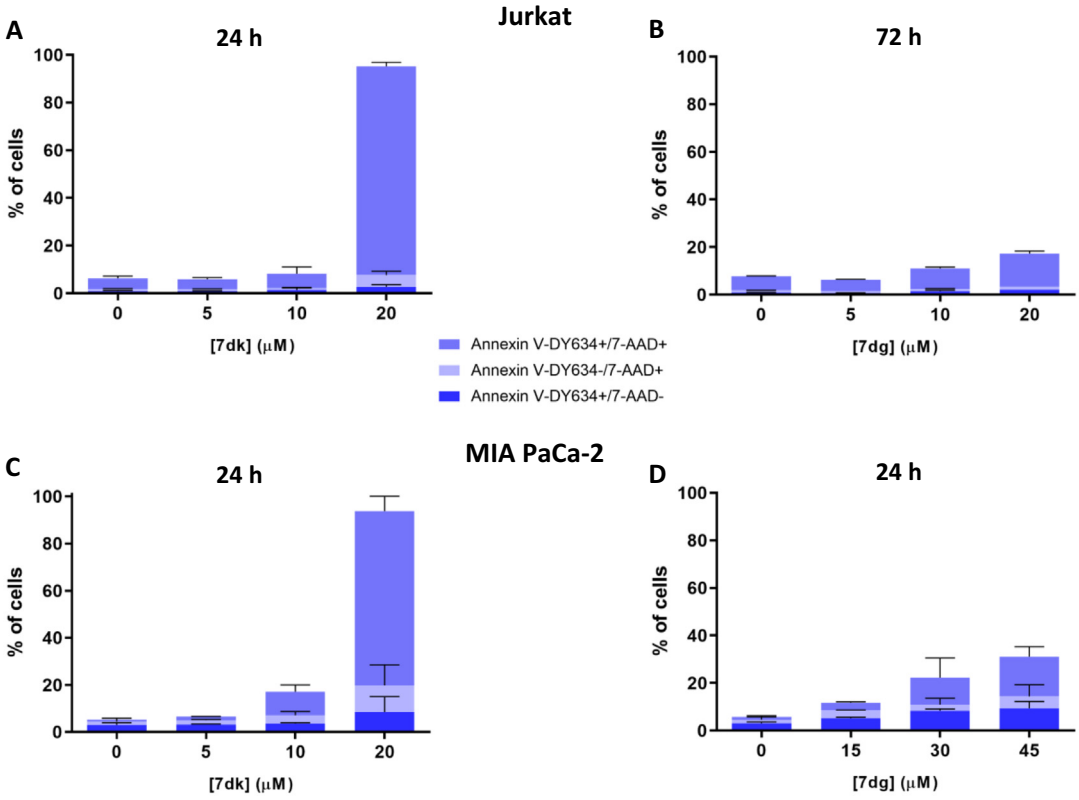

Fig. 9 Cytotoxic effect of **7dk** and **7dg** in Jurkat cells at 24 h (**A**) and at 72 h (**B**), respectively, and in MIA PaCa-2 cells at 24 h (**C** and **D**).

age to reduce the death induced by **7dg** in the pancreatic cell line (Fig. 11C).

Taken all this together, we gather that these compounds promote a caspase-independent cell death mechanism, but necroptosis is not activated in our models. In addition, the formation of many large vacuoles with **7dk** in MIA PaCa-2 cells leads us to suspect that an alternative cell death mechanism known as paraptosis could be activated in this case. One of the hallmarks of this novel form of programmed cell death is the massive cytoplasmic vacuolization resulting from the dilatation of the endoplasmic reticulum and, to a lesser extent, of the mitochondria, accompanied by the absence of caspase activity and apoptotic morphology (Wang et al., 2019). Although these features fit our results, typical apoptotic and necrotic morphologies are also observed under the microscope that are consistent with flow cytometry analysis (Figs. 8 and 9). This may mean that **7dk** is an extraordinary inducer of cell death in the pancreatic cell line, since it is capable of triggering three death pathways, although it is also possible that paraptosis ends up leading to apoptosis. In this sense, a study with an Alzheimer's disease cellular model proposes that during early pathological stages of the disease paraptosis befalls and when it progresses, the mitochondria are damaged, which provokes changes in the expression of the Bcl-2 family proteins leading to the activation of the mitochondrial apoptotic pathway (Jia et al., 2015). In any case, further studies are needed to unravel what happens at the molecular level in the presence of the tested DHPs derivatives. Since the only structural difference between both compounds is the substitution of a chloro group (**7dg**) by a CF_3 group (**7dk**) of one of the aromatic rings, it is possible that the particularities described for **7dk** are due to the presence of the CF_3 group, which has been shown to improve bioavailability (Shah and Westwell, 2007; Gillis et al., 2015). Notwithstanding, more in-depth studies are again required to confirm this hypothesis. Paraptosis has been related to naturally occurring compounds including curcumin, celastrol, hesperidin or cyclosporine A, as well as synthetic ones, i.e. benfotiamine and mainly metallic compounds containing rhenium, ruthenium, copper, iridium and titanium (Wang et al., 2019; Ye et al., 2015; Li et al., 2017; Tardito et al., 2011; Gandin et al., 2012; Yokoi et al., 2020; He et al; 2018; Cini et al., 2016). Likewise, it has also been described that sub-lethal doses of lercanidipine, a third-generation 1,4-dihydropyridine, induce paraptotic cell death in cancer cells resistant to proteasome inhibitors (Lee et al., 2019). However, to the best of our knowledge, there is no evidence that similar compounds to those used here unleash this type of cell death.

3.3.3. Mitochondrial transmembrane potential disruption

The pivotal role of mitochondria in cells is fully known. Considered the heart of cellular metabolism, they are the main players in the bioenergetics maintenance by supplying ATP to cells (Bock and Tait, 2020). In turn, they participate in many vital cell processes, such as the biosynthesis of several macromolecules, Ca^{2+}-homeostasis, gene expression, differentiation, inflammation and even cell death (Vakifahmetoglu-Norberg et al., 2017). In fact, its role in apoptosis has been thoroughly examined and its involvement in other types of programmed cell death has also been reported (Jeong and Seol, 2008). In these cases, the role of mitochondria is still

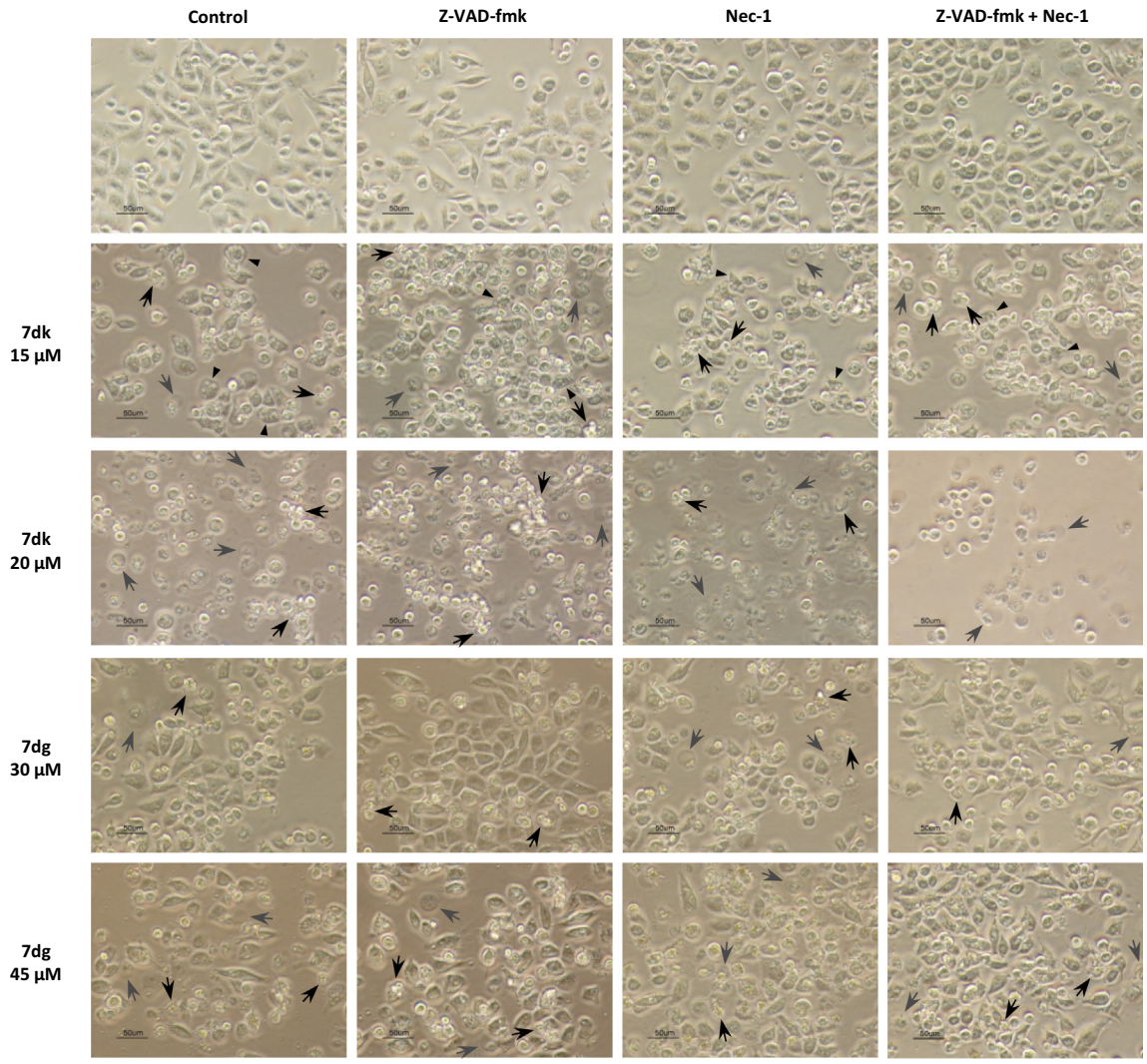

Fig. 10 Phase-contrast microscopy images of MIA PaCa-2 cells. Cells were preincubated for 1 h with 30 μM Z-VAD-fmk, Nec-1 or a combination of both prior to the addition of the compounds, which were incubated for 24 h. Black and grey arrows point to examples of apoptotic and necrotic cells, respectively. Little black triangles show cells containing cytoplasmic vacuoles.

not well understood but the idea that different modalities of cell death crosstalk one another and that this organelle act as a mediator is gaining strength (Bock and Tait, 2020). Thus, we focused on the mitochondria to conclude with the biological experiments.

Specifically, we evaluated the integrity of the outer mitochondrial membrane by flow cytometry using the TMRE (tetramethylrhodamine ethyl ester) probe. This molecule accumulates in active mitochondria, but certain cellular stresses, including chemotherapeutic agents, prompt mitochondrial outer membrane permeabilization (MOMP) and subsequent mitochondrial depolarization, which hinders TMRE incorporation. The obtained results demonstrate different effects on the mitochondrial potential depending on the cell line and the species incubated. Fig. 12A shows a complete disruption of mitochondrial transmembrane potential with the highest dose of **7dk** in Jurkat cells. Lower doses of this compound and **7dg** scarcely induce mitochondrial depolarization (Fig. 12: A and B). Interestingly, **7dg** at the highest concentration drives to partial mitochondrial membrane potential decrease and in turn to a slight hyperpolarization of those mitochondria that preserve their transmembrane potential (Fig. 12B). Contrariwise, the loss of the mitochondrial transmembrane potential is more evident in MIA PaCa-2 cells with all the treatments. Similar to Jurkat cells, the potential is utterly and dramatically lost with the highest and intermediate dose of **7dk**, respectively; however, the lowest concentration has little effect on mitochondrial potential (Fig. 13A). In the case of **7dg**, the disruption is moderate at the doses tested (Fig. 13B).

These results correlate with those of cytotoxicity, since generally MOMP, considered as an 'all-or-nothing' decision for cells, precedes PS exposure in the apoptotic process (Vorobjev, and Barteneva, 2015; Kalkavan and Green, 2018). Hence, the loss of mitochondrial transmembrane potential may be slightly higher than the recorded death. Nevertheless, the exception occurs in the MIA PaCa-2 cells with **7dk** at a dose of 10 μM, with which Annexin-V positive labeling is poor but, surprisingly, a noteworthy mitochondrial potential decrease befalls. This lay bare that other molecular mecha-

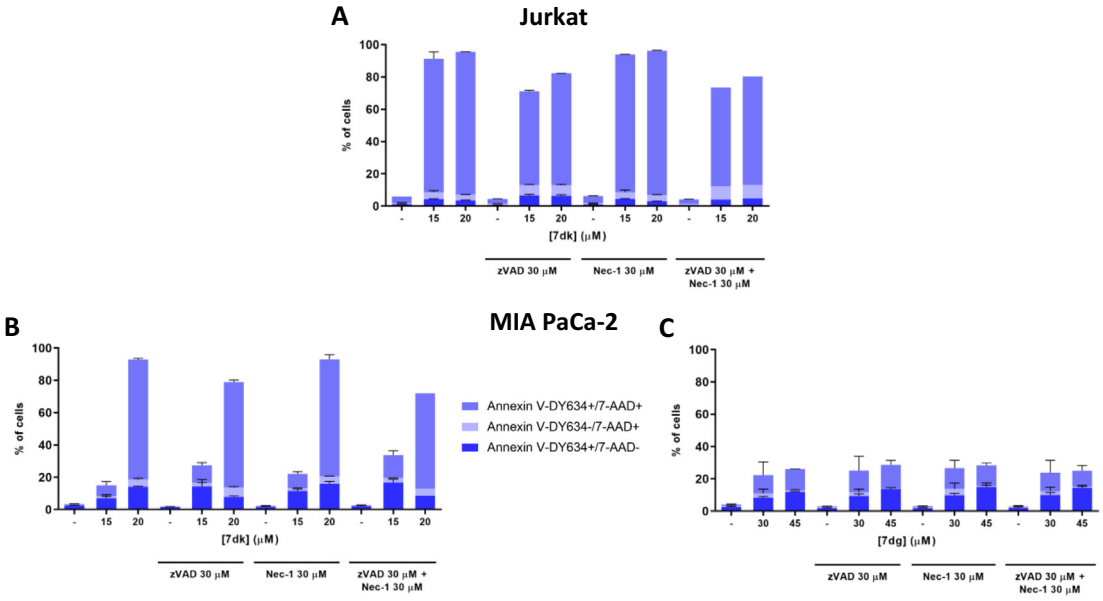

Fig. 11 Cell death mechanism triggered by **7dk** in Jurkat (**A**) and MIA PaCa-2 cells (**B**) and **7dg** in MIA PaCa-2 cells (**C**).

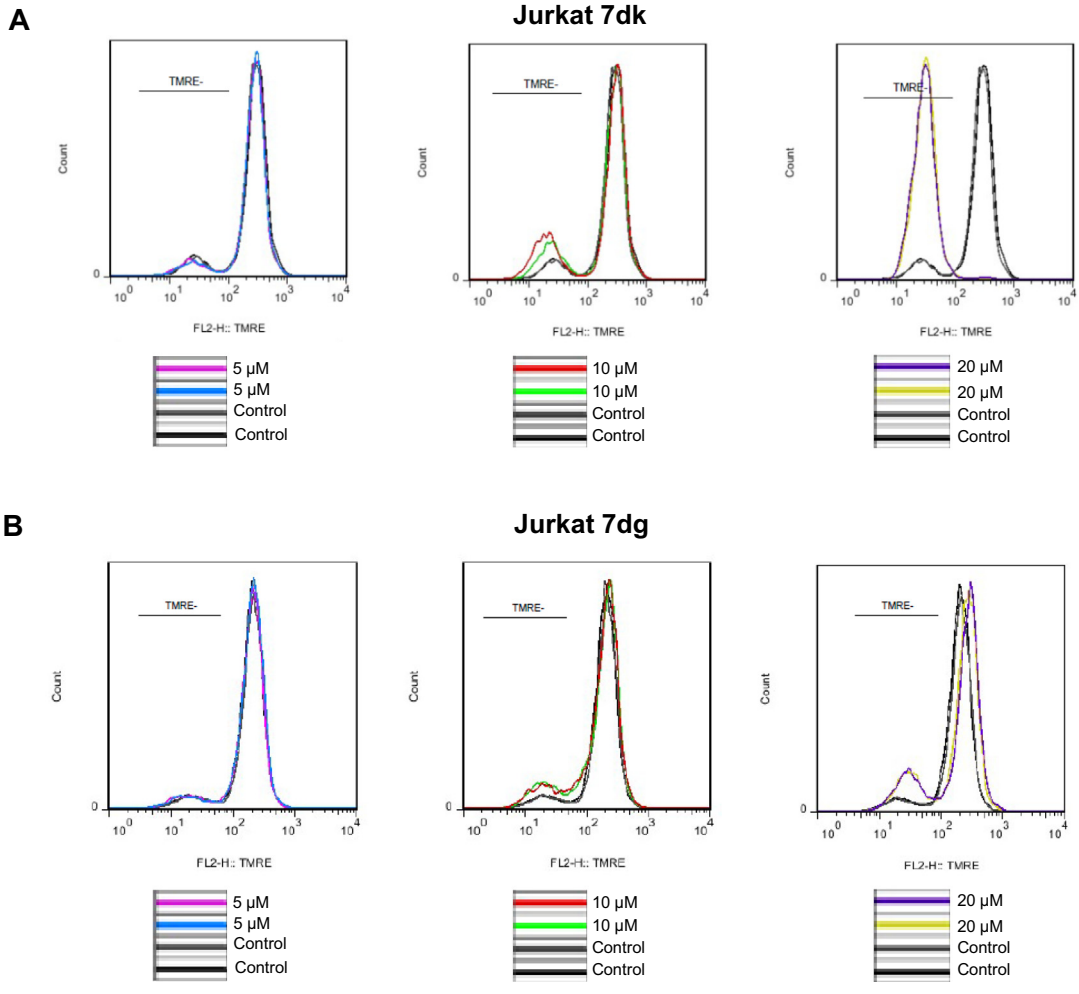

Fig. 12 Mitochondrial transmembrane potential disruption induced by **7dk** and **7dg** in Jurkat cells after 24 h of treatment.

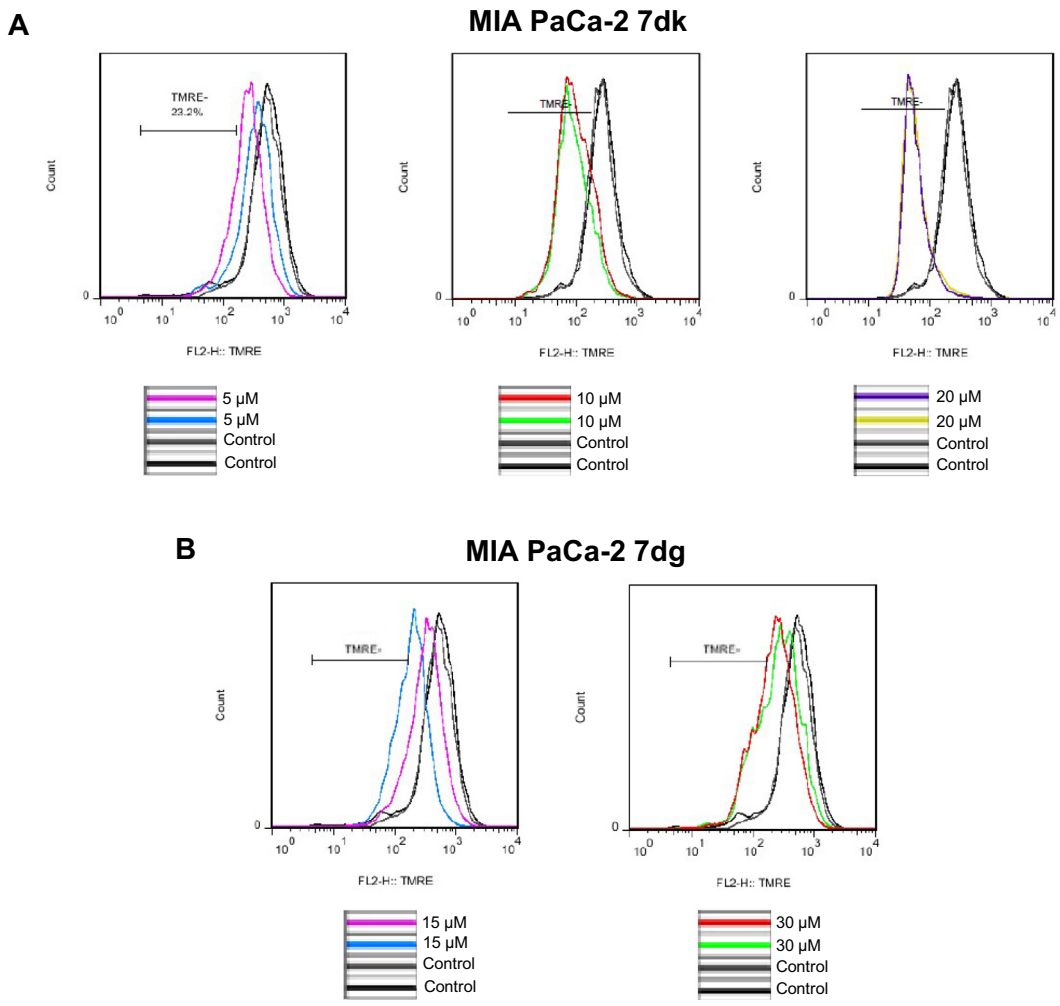

Fig. 13 Mitochondrial transmembrane potential disruption induced by **7dk** and **7dg** in MIA PaCa-2 cells after 24 h of treatment.

nisms different from apoptosis are involved and, as already mentioned above, paraptotic cell death cannot be ruled out.

3.4. Photophysical properties

Emissive properties of all 1,4-dihydropyridine derivatives were studied in DMSO solution in concentrations ranging from 1 to 5 mM. The emission and excitation maxima are collected in Tables 1 and 2. Most of the compounds were emissive revealing a maxima emission band between 400 and 506 nm. However, a thorough analysis revealed some relationship between the chemical structure and the emissive properties. Thus, strong dependence on the nature of the aromatic ring at the 1,4-dihydropyridine core seems to rule the capacity of the compound to emit light, see Table 1 and Figure S42.

On the base of the results reported in Table 1, some statements can be concluded. Thus, compounds containing a halogen substituted phenyl ring in *para* position at the alkylidene malononitrile reagent, i.e. 4-ClC_6H_4 (**7bg**), 4-BrC_6H_4 (**7bh**) were not emissive, which contrasts with the emission showed by **7be** centered at 450 nm, having a 3-ClC_6H_4. In addition, compounds with cyano and trifluoromethyl groups, 4-NCC_6H_4 (**7ai** and **7bi**) and 4-$F_3CC_6H_4$ (**7bk**), displayed an emission between 459 and 500 nm. In the case of nitrophenyl derivatives, 4-$O_2NC_6H_4$ (**7bf**) and 3-$O_2NC_6H_4$ (**7bd**), none of them were found emissive, following the same non-emissive behavior reported by Pávez and Encinas for similar nitrophenyl DHP (Pávez and Encinas, 2007). The most energetic emission band is observed for an electron donor substituted compound, **7bj** (4-MeC_6H_4), at 400 nm. An additional remark regarding the 1,4-dihydropyridine core was the blue shifted emission and the higher intensity delivered by **7ba** and **7bi** in comparison with that of their analogous **7aa** and **7ai**, being the only difference the substitution of the dicarboxylate residue, going from OEt (**7ba** and **7bi**) to OMe (**7aa** and **7ai**), see Table 1 and Fig. 14 (see also, in the supporting information, Figure S43). Surprisingly, compound **7bb**, containing a naphthyl group instead of the phenyl ring showed no emission. However, the thiophene derivative **7bc** displayed a strong luminescence centered at 506 nm.

Thereafter, the emissive properties for families of 1-benzamido-1,4-dihydropyridines **7bg-gg** (4-ClC_6H_4) and **7bk-gk** (4-$F_3CC_6H_4$) were analyzed separately in order to assess how the hydrazide functionalization might affect the photophysical behavior (Table 2 and Figure S43).

The most remarkable result was the higher emissive character of **7cg** and **7ck** in comparison with that of their counterparts. Both compounds containing the benzohydrazide

Table 1 Photophysical data of compounds derived from 1,4-dihydropyridine core (**7aa**, **7ai** and **7ba-bk**) recorded in DMSO solution (1–5 mM) at room temperature (298 K).

1,4-DHP	λ_{exc} (nm)	λ_{em} (nm)	R	1,4-DHP	λ_{exc} (nm)	λ_{em} (nm)	R
7aa	400	470	Ph	**7bg**	–	–	4-ClC_6H_4
7ba	375	433	Ph	**7bh**	–	–	4-BrC_6H_4
7bb	–	–	Naphthyl	**7ai**	419	500	4-NCC_6H_4
7bc	375	506	2-Thienyl	**7bi**	395	466	4-NCC_6H_4
7bd	–	–	3-$O_2NC_6H_4$	**7bj**	310	400	4-MeC_6H_4
7be	309	450	3-ClC_6H_4	**7bk**	395	459	4-$F_3CC_6H_4$
7bf	–	–	4-$O_2NC_6H_4$				

Table 2 Photophysical data of 1-benzamido-1,4-dihydropyridines **7bg-gg** and **7bk-gk** recorded in DMSO solution (1–5 mM) at room temperature (298 K).

1,4-DHP	λ_{exc} (nm)	λ_{em} (nm)	R	1,4-DHP	λ_{exc} (nm)	λ_{em} (nm)	R
7bg	–	–	Ph	**7bk**	395	459	Ph
7cg	478	529	$CH_2C_6H_5$	**7ck**	420,545	457,562	$CH_2C_6H_5$
7dg	–	–	-$(CH_2)_6CH_3$	**7dk**	305	450	-$(CH_2)_6CH_3$
7eg	–	–	4-$O_2NC_6H_4$	**7ek**	–	–	4-$O_2NC_6H_4$
7fg	429	504	4-ClC_6H_4	**7fk**	400	457	4-ClC_6H_4
7gg	426	508	4-$MeOC_6H_4$	**7gk**	377	451	4-$MeOC_6H_4$

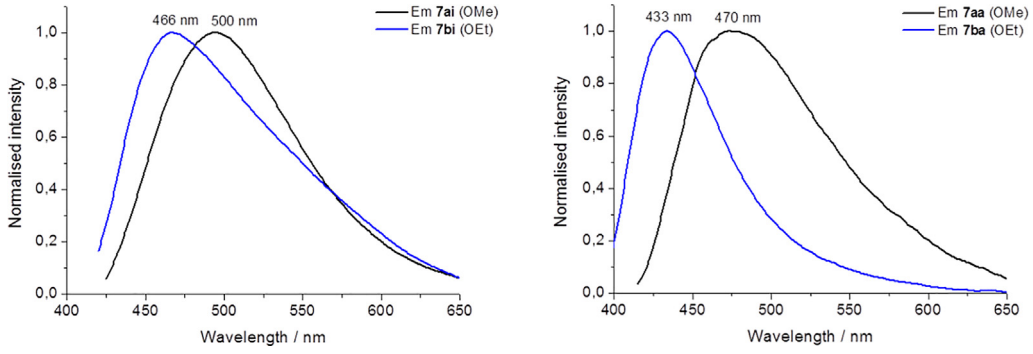

Fig. 14 Emission spectra of **7ai** and **7bi** (left) and **7aa** and **7ba** (right).

moiety displayed an emissive broad band center at 529 and 457 nm respectively. Moreover, **7ck** displayed an additional structured peak centered at 562 nm, when it is irradiated at lower energies, see Fig. 15. Contrary to those, compounds **7bg**, **7dg** and **7ek** were not emissive or were barely emissive like **7eg**. Moreover, the other compounds from the two families displayed low intense broad emissive bands between 450 and 508 nm.

Based on the maxima emission and excitation data found for analyzed compounds **7**, it can be concluded that **7cg** and **7ck** have good prospects within cell imaging applications. Their higher intensity emission in comparison with that of their counterparts, together with the lower energies needed for their photoactivation (over 470 nm) and the emission maxima over 500 nm, might be a good ally to overcome problems related to autofluorescence from biological samples, and thus increase the signal-to-noise ratio. This advantage would be especially important in the case of **7ck**, which could be excited at 545 nm, far away from the photoactivation of the biological material and rendering better quality bioimages.

3.5. In vivo assays

Finally, we also performed an *in vivo* toxicity study to evaluate the effect of two of the most active DHP derivatives. For such a purpose, compounds **7dg** and **7dk** were selected, both with the same heptyl substituent in the hydrazide moiety. In this study, an acute oral (PO) and intraperitoneal (IP) toxicity test were performed based on the OECD Test No. 425: Acute Oral Toxicity: Up-and-Down Procedure (Test, 2022). The highest dose tested was 17.5 mg/kg and the starting dose was 0.175 mg/kg, applying a slope of 2. The test was performed in male RjOrl: SWISS mice of 9–13 weeks with dosing intervals of 48 h. Then, toxicity was evaluated after a single administration.

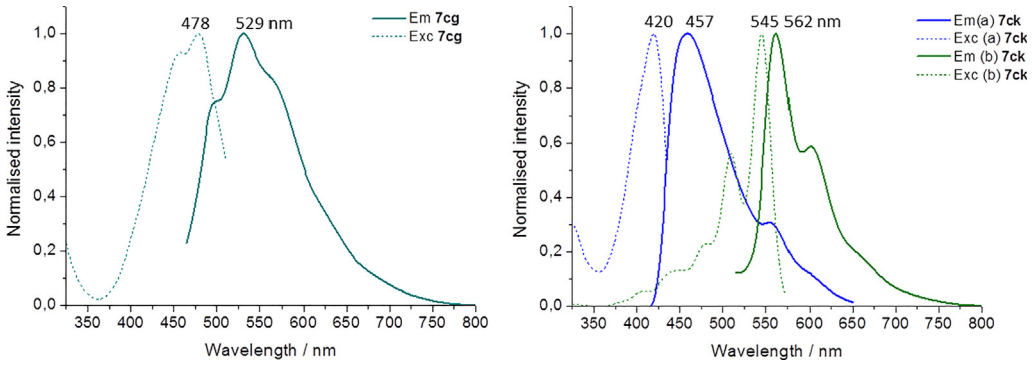

Fig. 15 Emission and excitation spectra of **7cg** (left) and **7ck** (right).

The solution of each tested compound was prepared in a DMSO (5 % max.): Water Milli-Q suspension and was administered in a volume of 1 mL/100 g of body weight. The animal health assessment was measured by weighing them and checking their general status through an evaluation scale (0–11 points) (Morton and Griffiths, 1985) during the whole process. These data were collected at 1, 2, 7 and 14 days and are reported in the supporting information of this article.

Interestingly, none of the animals showed significant weight variations at any of the times evaluated, both in the PO and IP tests. The variation of the weight was always < 5 % of loss with respect to the initial weight of the mice, for both tests at 24 and 48 h, respectively. The same occurs after one week or even two weeks, where is possible to observe just an increase in weight in agreement with the strain and sex of the animals (see Table S5 in the supporting information for all data).

Moreover, in both types of administration (PO and IP) no loss of animal welfare was detected in any of the mice during the 14 days after the administration of the products (zero value in the evaluation scale of all animals on 1, 2, 7 and 14 days). It is worth mentioning that the administered doses to the mice were around 2500 and 3300 times more concentrated than the IC_{50} values for **7dg** and **7dk**, respectively, in *in vitro* assays, and that none of the animals died with any dose supplied in each of the two groups of substances. These studies support the lack of toxicity of the tested 1,4-DHPs in non-cancer cells or at least, their major specificity for cancer cells. This property could open the door to further efficacy studies using these DHPs in other *in vivo* tests for the discovery of new potential anticancer drugs.

4. Conclusions

A new family of 1,4-DHPs bearing a hydrazide moiety has been successfully synthesized with moderate to excellent yields.

These 1,4-DHPs have been tested against HeLa, Jurkat, A549 and MIA PaCa-2 cancer cell lines, showing good activity. The first structure–activity assessment related to the aryl group of our compounds has indicated that the 4-Cl substituted structure **7bg** is the best candidate overall. This product, together with a 4-CF_3 substituted one **7bk**, due to similitude and enhanced biocompatibility, have been used as models to create a second generation of molecules modifying their *N*-heterocyclic position. 4-CF_3 substituted compounds have provided the best results, with IC_{50} values close to the nM range. Interestingly, these results can be improved at longer incubation times, making these compounds good candidates to perform more specific studies.

Under the microscope, cells show apoptotic and necrotic morphologies upon exposure to the compounds, and flow cytometry assays support these observations in different cases. Moreover, a more detailed labeled experiment together with mitochondrial transmembrane potential disruption measurements suggest that our compounds trigger a non-conventional caspase-independent cell death mechanism known as paraptosis.

Concerning the photophysical properties of our compounds, some of them show intense excitations and emissions at relatively high wavelengths (green to yellow) which could be of great use to develop new biomarkers and theragnostic agents.

Finally, acute oral toxicity tests in mice show that dosing extraordinarily high concentrations (2500 to 3300 times the IC_{50} values) of our test compound does not produce any adverse effect on the specimens for at least two weeks, which indicates a lack of toxicity or at least a major selectivity to cancerous cells. These results support further studies and optimizations so as to better understand the behavior of these promising compounds.

Research funding

This research was funded by Agencia Estatal de Investigación (AEI), project PID2019-104379RB-C21 and PID2020-117455 GB-I00/AEI/10.13039/501100011033; RED2018-102471-T (MCIN/ AEI/10.13039/501100011033), RTI2018-097836-J-I00 (MCIN/AEI/10.13039/501100011033/FEDER), RYC2018-025872-I (MCIN/AEI/10.13039/501100011033), by "ESF Investing in your future" and Gobierno de Aragón-Fondo Social Europeo (Research Groups E07_20R and B31_20R).

Declaration of competing interest

The authors declare that they have no known competing financial interests or personal relationships that could have appeared to influence the work reported in this paper.

Acknowledgements

The authors thank Agencia Estatal de Investigación (AEI), project PID2019-104379RB-C21 and PID2020-117455GB-I00 /AEI/10.13039/501100011033; RED2018-102471-T (MCIN/AEI/10.13039/501100011033), RTI2018-097836-J-I00 (MCIN/AEI/10.13039/501100011033/FEDER), RYC2018-025872-I (MCIN/AEI/10.13039/501100011033), by "ESF Investing in your future" and Gobierno de Aragón-Fondo Social Europeo (Research Groups E07_20R and B31_20R) for financial sup-

port of this research. S. A. thanks the DGA (Aragon Government) for a predoctoral fellowship.

Appendix A. Supplementary material

Supplementary data related to this article can be found at http://dx.doi.org/. These data include synthetic procedures of precursors **3** and **6** and excitation and emission spectra of 1,4-dihydropyridine derivatives **7**, as well as copies of the ^{1}H and $^{13}C\{^{1}H\}$-APT NMR spectra of all new compounds. The supporting information also reports the biological section related to IC_{50} values and *in vivo* assays with mice. Supplementary data to this article can be found online at https://doi.org/10.1016/j.arabjc.2022.104514.

References

Abbas, H.-A.-S., El Sayed, W.A., Fathy, N.M., 2010. Synthesis and antitumor activity of new dihydropyridine thioglycosides and their corresponding dehydrogenated forms. Eur. J. Med. Chem. 45, 973–982. https://doi.org/10.1016/j.ejmech.2009.11.039.

Alexiou, C., Schmid, R.J., Jurgons, R., Kremer, M., Wanner, G., Bergemann, C., Huenges, E., Nawroth, T., Arnold, W., Parak, F. G., 2006. Targeting cancer cells: magnetic nanoparticles as drug carriers. Eur. Biophy. J. 35, 446–450. https://doi.org/10.1007/s00249-006-0042-1.

Auria-Luna, F., Marqués-López, E., Mohammadi, S., Heiran, R., Herrera, R.P., 2015. New organocatalytic asymmetric synthesis of highly substituted chiral 2-oxospiro-[indole-3,4′-(1′,4′-dihydropyridine)] derivatives. Molecules 20, 15807–15826. https://doi.org/10.3390/molecules200915807.

Auria-Luna, F., Marqués-López, E., Gimeno, M.C., Heiran, R., Mohammadi, S., Herrera, R.P., 2017. Asymmetric organocatalytic synthesis of substituted chiral 1,4-dihydropyridine derivatives. J. Org. Chem. 82, 5516–5523. https://doi.org/10.1021/acs.joc.7b00176.

Auria-Luna, F., Marqués-López, E., Herrera, R.P., 2018. First organocatalytic asymmetric synthesis of 1-benzamido-1,4-dihydropyridine derivatives. Molecules 23, 2692. https://doi.org/10.3390/molecules23102692.

Auria-Luna, F., Marqués-López, E., Romanos, E., Fernández-Moreira, V., Gimeno, M.C., Marzo, I., Herrera, R.P., 2020. Novel ureido-dihydropyridine scaffolds as theranostic agents. Bioorg. Chem. 105. 104364. https://doi.org/10.1016/j.bioorg.2020.104364.

Azzam, R.A., Mohareb, R.M., 2015. Multicomponent reactions of acetoacetanilide derivatives with aromatic aldehydes and cyanomethylene reagents to produce 4*H*-pyran and 1,4-dihydropyridine derivatives with antitumor activities. Chem. Pharm. Bull. 63, 1055–1064. https://doi.org/10.1248/cpb.c15-00685.

Bazargan, L., Fouladdel, S., Shafiee, A., Amini, M., Ghaffari, S.M., Azizi, E., 2008. Evaluation of anticancer effects of newly synthesized dihydropyridine derivatives in comparison to verapamil and doxorubicin on T47D parental and resistant cell lines *in vitro*. Cell Biol. Toxicol. 24, 165–174. https://doi.org/10.1007/s10565-007-9026-x.

Bock, F.J., Tait, S.W.G., 2020. Mitochondria as multifaceted regulators of cell death. Nat. Rev. Mol. Cell Biol. 21, 85–100. https://doi.org/10.1038/s41580-019-0173-8.

Bray, F., Laversanne, M., Weiderpass, E., Soerjomataram, I., 2021. The ever-increasing importance of cancer as a leading cause of premature death worldwide. Cancer 127, 3029–3030. https://doi.org/10.1002/cncr.33587.

Bruijnincx, P.C.A., Sadler, P.J., 2008. New trends for metal complexes with anticancer activity. Curr. Op. Chem. Bio. 12, 197–206. https://doi.org/10.1016/j.cbpa.2007.11.013.

Bruncko, M., 2012. Dihydropyridine-based calcium channel blockers for the treatment of angina pectoris and hypertension. In: Lamberth, C., Dinges, J. (Eds.), Bioactive Heterocyclic Compound Classes: Pharmaceuticals. Wiley-VCH, Verlag, pp. 135–151.

Carosati, E., Ioan, P., Micucci, M., Broccatelli, F., Cruciani, G., Zhorov, B.S., Chiarini, A., Budriesi, R., 2012. 1,4-Dihydropyridine scaffold in medicinal chemistry, the story so far and perspectives (part 2): action in other targets and antitargets. Curr. Med. Chem. 19, 4306–4323. https://doi.org/10.2174/092986712802884204.

Chhillar, A.K., Arya, P., Mukherjee, C., Kumar, P., Yadav, Y., Sharma, A.K., Yadav, V., Gupta, J., Dabur, R., Jha, H.N., Watterson, A.C., Parmar, V.S., Prasad, A.K., Sharma, G.L., 2006. Microwave-assisted synthesis of antimicrobial dihydropyridines and tetrahydropyrimidin-2-ones: novel compounds against aspergillosis. Bioorg. Med. Chem. 14, 973–981. https://doi.org/10.1016/j.bmc.2005.09.014.

Cini, M., Williams, H., Fay, M.W., Searle, M.S., Woodward, S., Bradshaw, T.D., 2016. Enantiopure titanocene complexes – direct evidence for paraptosis in cancer cells. Metallomics 8, 286–297. https://doi.org/10.1039/c5mt00297d.

Cuciniello, R., Filosa, S., Crispi, S., 2021. Novel approaches in cancer treatment: preclinical and clinical development of small non-coding RNA therapeutics. J. Exp. Clin. Can. Res. 40, 383. https://doi.org/10.1186/s13046-021-02193-1.

Dhankhar, R., Kawatra, A., Mohanty, A., Gulati, P., 2021. Microbial enzymes used in prodrug activation for cancer therapy: insights and future perspectives. Curr. Prot. Pept. Scie. 22, 514–525. https://doi.org/10.2174/1389203721666201207231932.

Dhinakaran, I., Padmini, V., Bhuvanesh, N., 2015. One-pot synthesis of *N*-aryl 1,4-dihydropyridine derivatives and their biological activities. J. Chem. Sci. 127, 2201–2209. https://doi.org/10.1007/s12039-015-0983-y.

Dunai, Z.A., Imre, G., Barna, G., Korcsmaros, T., Petak, I., Bauer, P. I., Mihalik, R., 2012. Staurosporine induces necroptotic cell death under caspase-compromised conditions in U937 cells. PLoS ONE 7, e41945.

Edraki, N., Mehdipour, A.R., Khoshneviszadeh, M., Miri, R., 2009. Dihydropyridines: evaluation of their current and future pharmacological applications. Drug Discov. Today 14, 1058–1066. https://doi.org/10.1016/j.drudis.2009.08.004.

Fernández-Moreira, V., Gimeno, M.C., 2018. Heterobimetallic complexes for theranostic applications. Chem. Eur. J. 24, 3345–3353. https://doi.org/10.1002/chem.201705335.

Fernández-Moreira, V., Sastre-Martín, H., 2017. Photophysical and bioactivity behavior of fac-rhenium(I) derivatives containing ditopic sulfurpyridine ligands. Inorg. Chim. Acta 460, 127–133. https://doi.org/10.1016/j.ica.2016.07.038.

Fernández-Moreira, V., Marzo, I., Gimeno, M.C., 2014. Luminescent Re(I) and Re(I)/Au(I) complexes as cooperative partners in cell imaging and cancer therapy. Chem. Sci. 5, 4434–4446. https://doi.org/10.1039/C4SC01684J.

Fernández-Moreira, V., Alegre-Requena, J.V., Herrera, R.P., Marzo, I., Gimeno, M.C., 2016. Synthesis of luminescent squaramide monoesters: cytotoxicity and cell imaging studies in HeLa cells. RSC Adv. 6, 14171–14177. https://doi.org/10.1039/C5RA24521D.

Fernández-Moreira, V., Herrera, R.P., Gimeno, M.C., 2019a. Anticancer properties of gold complexes with biologically relevant ligands. Pure Appl. Chem. 91, 247–269. https://doi.org/10.1515/pac-2018-0901.

Fernández-Moreira, V., Val-Campillo, C., Ospino, I., Herrera, R.P., Marzo, I., Laguna, A., Gimeno, M.C., 2019b. Bioactive and luminescent indole and isatin based gold(I) derivatives. Dalton Trans. 48, 3098–3108. https://doi.org/10.1039/C8DT00298C.

Firuzi, O., Javidnia, K., Mansourabadi, E., Saso, L., Mehdipour, A. R., Miri, R., 2013. Reversal of multidrug resistance in cancer cells by novel asymmetrical 1,4-dihydropyridines. Arch. Pharm. Res. 36, 1392–1402. https://doi.org/10.1007/s12272-013-0149-8.

Gadotti, V.M., Bladen, C., Zhang, F.X., Chen, L., Gündüz, M.G., Şimşek, R., Şafak, C., Zamponi, G.W., 2015. Analgesic effect of a broad-spectrum dihydropyridine inhibitor of voltage-gated calcium channels. Pflug. Arch. – Eur. J. Physiol. 467, 2485–2493. https://doi.org/10.1007/s00424-015-1725-1.

Gandin, V., Pellei, M., Tisato, F., Porchia, M., Santini, C., Marzano, C., 2012. A novel copper complex induces paraptosis in colon cancer cells via the activation of ER stress signalling. J. Cell. Mol. Med. 16, 142–151. https://doi.org/10.1111/j.1582-4934.2011.01292.x.

Gillis, E.P., Eastman, K.J., Hill, M.D., Donnelly, D.J., Meanwell, N. A., 2015. Applications of fluorine in medicinal chemistry. J. Med. Chem. 58, 8315–8359. https://doi.org/10.1021/acs.jmedchem.5b00258.

Goitia, H., Nieto, Y., Villacampa, M.D., Casper, C., Laguna, A., Gimeno, M.C., 2013. Antitumoral gold and silver complexes with ferrocenyl-amide phosphines. Organometallics 32, 6069–6078. https://doi.org/10.1021/om400633z.

Gómez-Galeno, J.E., Hurtado, C., Cheng, J., Yardimci, C., Mercola, M., Cashman, J.R., 2018. *b*-Annulated 1,4-dihydropyridines as Notch inhibitors. Bioorg. Med. Chem. Lett. 28, 3363–3367. https://doi.org/10.1016/j.bmcl.2018.09.002.

Goto, R.N., Sobral, L.M., Sousa, L.O., Garcia, C.B., Lopes, N.P., Marín-Prida, J., Ochoa-Rodríguez, E., Verdecia-Reyes, Y., Pardo-Andreu, G.L., Curti, C., Leopoldino, A.M., 2018. Anti-cancer activity of a new dihydropyridine derivative, VdiE-2N, in head and neck squamous cell carcinoma. Eur. J. Pharmacol. 819, 198–206. https://doi.org/10.1016/j.ejphar.2017.12.009.

Griendling, K.K., Minieri, C.A., Ollerenshaw, J.D., Alexander, R.W., 1994. Angiotensin II stimulates NADH and NADPH oxidase activity in cultured vascular smooth muscle cells. Circ. Res. 74, 1141–1148. https://doi.org/10.1161/01.RES.74.6.1141.

Gutiérrez, A., Gracia-Fleta, L., Marzo, I., Cativiela, C., Laguna, A., Gimeno, M.C., 2014. Gold (I) thiolates containing amino acid moieties. cytotoxicity and structure–activity relationship studies. Dalton Trans. 43, 17054–17066. https://doi.org/10.1039/C4DT02299H.

Gutiérrez, A., Marzo, I., Cativiela, C., Laguna, A., Gimeno, M.C., 2015. Highly cytotoxic bioconjugated gold(I) complexes with cysteine-containing dipeptides. Chem. Eur. J. 21, 11088–11095. https://doi.org/10.1002/chem.201501458.

Hadizadeh, F., Rahimi, B., Taghiabadi, E., Razavi, M., Karimi, G., 2013. Evaluation of anticonvulsant effect of two novels 4-[1-(4-fluorobenzyl)-5-imidazolyl] dihydropyridine derivatives in mice. Res. Pharm. Sci. 8, 91–95.

Hantzsch, A., 1881. Condensationsprodukte aus Aldehydammoniak und ketonartigen Verbindungen. Ber. Dtsch. Chem. Ges. 14, 1637–1638. https://doi.org/10.1002/cber.18810140214.

He, L., Wang, K.-N., Zheng, Y., Cao, J.-J., Zhang, M.-F., Tan, C.-P., Ji, L.-N., Mao, Z.-W., 2018. Cyclometalated iridium(III) complexes induce mitochondria-derived paraptotic cell death and inhibit tumor growth *in vivo*. Dalton Trans. 47, 6942–6953. https://doi.org/10.1039/C8DT00783G.

Hilgeroth, A., 2002. Dimeric 4-aryl-1,4-dihydropyridines: development of a third class of nonpeptidic HIV-1 protease inhibitors. Mini-Rev. Med. Chem. 2, 235–245. https://doi.org/10.2174/1389557023406241.

Idhayadhulla, A., Kumar, R.S., Nasser, A.J.A., Kavamani, S., Indhumathy, S., 2015. Anti-inflammatory activity of new series of 1,4-dihydropyridine derivatives. Pharm. Chem. J. 49, 463–466. https://doi.org/10.1007/s11094-015-1305-x.

Indumathi, S., Karthikeyan, R., Nasser, A.J.A., Idhayadhulla, A., Kumar, R.S., 2015. Anticonvulsant, analgesic and anti-inflammatory activities of some novel pyrrole and 1,4-dihydropyridine derivatives. J. Chem. Pharm. Res. 7, 434–440.

Ioan, P., Carosati, E., Micucci, M., Cruciani, G., Broccatelli, F., Zhorov, B.S., Chiarini, A., Budriesi, R., 2011. 1,4-Dihydropyridine scaffold in medicinal chemistry, the story so far and perspectives (Part 1): action in ion channels and GPCRs. Curr. Med. Chem. 18, 4901–4922. https://doi.org/10.2174/092986711797535173.

Jeong, S.-Y., Seol, D.-W., 2008. The role of mitochondria in apoptosis. BMB Reports 41, 11–22. https://doi.org/10.5483/BMBRep.2008.41.1.011.

Jia, D.-P., Wang, S., Zhang, B.-C., Fang, F., 2015. Paraptosis triggers mitochondrial pathway-mediated apoptosis in Alzheimer's disease. Exp. Ther. Med. 10, 804–808. https://doi.org/10.3892/etm.2015.2531.

Kalkavan, H., Green, D.R., 2018. MOMP, cell suicide as a BCL-2 family business. Cell Death Diff. 25, 46–55. https://doi.org/10.1038/cdd.2017.179.

Lee, A.R., Seo, M.J., Kim, J., Lee, D.M., Kim, I.Y., Yoon, M.J., Hoon, H., Choi, K.S., 2019. Lercanidipine synergistically enhances bortezomib cytotoxicity in cancer cells via enhanced endoplasmic reticulum stress and mitochondrial Ca^{2+} overload. Int. J. Mol. Sci. 20, 6112. https://doi.org/10.3390/ijms20246112.

Li, C., Ip, K.-W., Man, W.-L., Song, D., He, M.-L., Yiu, S.-M., Lau, T.-C., Zhu, G., 2017. Cytotoxic (salen)ruthenium(II) anticancer complexes exhibit different modes of cell death directed by axial ligands. Chem. Sci. 8, 6865–6870. https://doi.org/10.1039/C7SC02205K.

Liu, Y., Fiskum, G., Schubert, D., 2002. Generation of reactive oxygen species by the mitochondrial electron transport chain. J. Neurochem. 80, 780–787. https://doi.org/10.1046/j.0022-3042.2002.00744.x.

Loev, B., Goodman, M., Snader, K., Tedeschi, R., Macko, E., 1974. Hantzsch-type dihydropyridine hypotensive agents. J. Med. Chem. 17, 956–965. https://doi.org/10.1021/jm00255a010.

Luengo, A., Fernández-Moreira, V., Marzo, I., Gimeno, M.C., 2017. Trackable metallodrugs combining luminescent Re(I) and bioactive Au(I) fragments. Inorg. Chem. 56, 15159–15170. https://doi.org/10.1021/acs.inorgchem.7b02470.

Mai, A., Valente, S., Meade, S., Carafa, V., Tardugno, M., Nebbioso, A., Galmozzi, A., Mitro, N., Fabiani, E.D., Altucci, L., Kazantsev, A., 2009. Study of 1,4-dihydropyridine structural scaffold: discovery of novel sirtuin activators and inhibitors. J. Med. Chem. 52, 5496–5504. https://doi.org/10.1021/jm9008289.

Mehta, P., Verma, P., 2013. Antimicrobial activity of some derivatives of 1,4-dihydropyridines. J. Chem. 2. 865128. https://doi.org/10.1155/2013/865128.

Milkovic, L., Vukovic, T., Zarkovic, N., Tatzber, F., Bisenieks, E., Kalme, Z., Bruvere, I., Ogle, Z., Poikans, J., Velena, A., Duburs, G., 2018. Antioxidative 1,4-dihydropyridine derivatives modulate oxidative stress and growth of human osteoblast-like cells *in vitro*. Antioxidants 7, 123. https://doi.org/10.3390/antiox7090123.

Montanel-Pérez, S., Herrera, R.P., Laguna, A., Villacampa, M.D., Gimeno, M.C., 2015. The fluxional amine gold(III) complex as an excellent catalyst and precursor of biologically active acyclic carbenes. Dalton Trans. 44, 9052–9062. https://doi.org/10.1039/C5DT00703H.

Morshed, S.R.M.D., Hashimoto, K., Murotani, Y., Kawase, M., Shah, A., Satoh, K., Kikuchi, H., Nishikawa, H., Maki, J., Sakagami, H., 2005. Tumor-specific cytotoxicity of 3,5-dibenzoyl-1,4-dihydropyridines. Anticancer Res. 25, 2033–2038.

Morton, D.B., Griffiths, P.H., 1985. Guidelines on the recognition of pain, distress and discomfort in experimental animals and a hypothesis for assessment. Vet. Rec. 116, 431–436. https://doi.org/10.1136/vr.116.16.431.

Olejníková, P., Švorc, L., Olšovská, D., Panáková, A., Vihonská, Z., Kovaryová, K., Marchalín, Š., 2014. Antimicrobial activity of novel C2-substituted 1,4-dihydropyridine analogues. Sci. Pharm. 82, 221–232. https://doi.org/10.3797/scipharm.1311-04.

Ortego, L., Meireles, M., Kasper, C., Laguna, A., Villacampa, M.D., Gimeno, M.C., 2016. Group 11 complexes with amino acid derivatives: Synthesis and antitumoral studies. J. Inorg. Biochem. 156, 133–144. https://doi.org/10.1016/j.jinorgbio.2015.12.018.

Pávez, P., Encinas, M.V., 2007. Photophysics and photochemical studies of 1,4-ihydropyridine derivatives. Photochem. Photobiol. 83, 722–729. https://doi.org/10.1562/2006-05-22-ra-898.

Pham, H.T., Chataigner, I., Renaud, J.-L., 2012. New approaches to nitrogen containing heterocycles: enantioselective organocatalyzed synthesis of dihydropyridines (DHP's), quinolizidine derivatives and dihydropyrimidines (DHPM's). Curr. Org. Chem. 16, 1754–1775. https://doi.org/10.2174/138527212802651322.

Pollak, N., Dölle, C., Ziegler, M., 2007. The power to reduce: pyridine nucleotides – small molecules with a multitude of functions. Biochem. J. 402, 205–218. https://doi.org/10.1042/BJ20061638.

Prabahar, K., Alanazi, Z., Qushawy, M., 2021. Targeted drug delivery system: advantages, carriers and strategies. Ind. J. Pharm. Ed. Res. 55, 346–353. https://doi.org/10.5530/ijper.55.2.72.

Quintana, M., Alegre-Requena, J.V., Marqués-López, E., Herrera, R. P., Triola, G., 2016. Squaramides with cytotoxic activity against human gastric carcinoma cells HGC-27: synthesis and mechanism of action. Med. Chem. Commun. 7, 550–561. https://doi.org/10.1039/C5MD00515A.

Ramírez-San Juan, E., Soriano-Ursúa, M.A., Espinosa-Raya, J., Correa-Basurto, J., Trujillo-Ferrara, J.G., Miranda-Ruvalcaba, R., Delgado-Reyes, F., Gómez-Pliego, R., 2014. Anticonvulsant effects of bis-1,4-dihydropyridines and the probable role of L-type calcium channels suggested by docking simulations. Med. Chem. Res. 23, 5149–5159. https://doi.org/10.1007/s00044-014-1083-0.

Reddy, G.M., Shiradkar, M., Chakravarthy, A.K., 2007. Chemical and Pharmacological Significance of 1,4-Dihydropyridines. Curr. Org. Chem. 11, 847–852. https://doi.org/10.2174/138527207781024058.

Sadowski-Debbing, K., Coy, J.F., Mier, W., Hug, H., Los, M., 2002. Caspases – their role in apoptosis and other physiological processes as revealed by knock-out studies. Arch. Immunol. Ther. Exp. 50, 19–34.

Safak, C., Simsek, R., 2006. Fused 1,4-dihydropyridines as potential calcium modulatory compounds. Mini Rev. Med. Chem. 6, 747–755. https://doi.org/10.2174/138955706777698606.

Saini, A., Kumar, S., Sandhu, J.S., 2008. Hantzsch reaction: recent advances in Hantzsch 1,4-dihydropyridines. J. Sci. Ind. Res. 67, 95–111 http://hdl.handle.net/123456789/753.

Salari, N., Rasoulpoor, S., Valipour, E., Mansouri, K., Bartina, Y., Dokaneheifard, S., Mohammadi, M., Abam, F. Liposomes, new carriers for delivery of genes and anticancer drugs: a systematic review. Anti-Cancer Drugs 33, e9–e20. https://doi.org/10.1097/cad.0000000000001144.

Salvador-Gil, D., Ortego, L., Herrera, R.P., Marzo, I., Gimeno, M.C., 2017. Highly active group 11 metal complexes with α-hydrazidophosphonate ligands. Dalton Trans. 46, 13745–13755. https://doi.org/10.1039/c7dt02743e.

Shah, P., Westwell, A.D., 2007. The role of fluorine in medicinal chemistry. J. Enzyme Inhib. Med. Chem. 22, 527–540. https://doi.org/10.1080/14756360701425014.

Sharma, V.K., Singh, S.K., 2017. Synthesis, utility and medicinal importance of 1,2- & 1,4-dihydropyridines. RSC Adv. 7, 2682–2732. https://doi.org/10.1039/C6RA24823C.

Shekari, F., Sadeghpour, H., Javidnia, K., Saso, L., Nazari, F., Firuzi, O., Miri, R., 2015. Cytotoxic and multidrug resistance reversal activities of novel 1,4-dihydropyridines against human cancer cells. Eur. J. Pharm. 746, 233–244. https://doi.org/10.1016/j.ejphar.2014.10.058.

Sirisha, K., Achaiah, G., Reddy, V.M., 2010. Facile synthesis and antibacterial, antitubercular, and anticancer activities of novel 1,4-dihydropyridines. Arch. Pharm. Chem. Life Sci. 243, 342–352. https://doi.org/10.1002/ardp.200900243.

Sirisha, K., Bikshapathi, D., Achaiah, G., Reddy, V.M., 2011. Synthesis, antibacterial and antimycobacterial activities of some new 4-aryl/heteroaryl-2,6-dimethyl-3,5-bis-*N*-(aryl)-carbamoyl-1,4-dihydropyridines. Eur. J. Med. Chem. 46, 1564–1571. https://doi.org/10.1016/j.ejmech.2011.02.003.

Stojak, M., Mazur, L., Opydo-Chanek, M., Łukawska, M., Oszczapowicz, I., 2013. *In vitro* induction of apoptosis and necrosis by new derivatives of daunorubicin. Anticancer Res. 33, 4439–4443.

Talwan, P., Chaudhary, S., Kumar, K., Rawal, R.K., 2017. Chemical and medical versatility of substituted 1,4-dihydropyridines. Curr. Bio. Comp. 13, 109–120. https://doi.org/10.2174/1573407212666160607090202.

Tardito, S., Bassanetti, I., Bignardi, C., Elviri, L., Tegoni, M., Mucchino, C., Bussolati, O., Franchi-Gazzola, R., Marchiò, L., 2011. Copper binding agents acting as copper ionophores lead to caspase inhibition and paraptotic cell death in human cancer cells. J. Am. Chem. Soc. 133, 6235–6242. https://doi.org/10.1021/ja109413c.

Test No. 425: Acute Oral Toxicity: Up-and-Down Procedure, 2022. https://www.oecd.org/env/test-no-425-acute-oral-toxicity-up-and-down-procedure-9789264071049-en.htm (accessed 16th march 2022).

Vakifahmetoglu-Norberg, H., Ouchida, A.T., Norberg, E., 2017. The role of mitochondria in metabolism and cell death. Biochem. Biophys. Res. Commun. 482, 426–431. https://doi.org/10.1016/j.bbrc.2016.11.088.

van Meerloo, J., Kaspers, G.J., Cloos, J., 2011. Cell sensitivity assays: the MTT assay. Methods Mol. Biol. 731, 237–245. https://doi.org/10.1007/978-1-61779-080-5_20.

Visbal, R., Fernández-Moreira, V., Marzo, I., Laguna, A., Gimeno, M.C., 2016. Cytotoxicity and biodistribution studies of luminescent Au(I) and Ag(I) *N*-heterocyclic carbenes. searching for new biological targets. Dalton Trans. 45, 15026–15033. https://doi.org/10.1039/C6DT02878K.

Voigt, B., Coburger, C., Monár, J., Hilgeroth, A., 2007. Structure–activity relationships of novel *N*-acyloxy-1,4-dihydropyridines as *P*-glycoprotein inhibitors. Bioorg. Med. Chem. 15, 5110–5113. https://doi.org/10.1016/j.bmc.2007.05.036.

Vorobjev, I., Barteneva, N., 2015. Temporal heterogeneity metrics in apoptosis induced by anticancer drugs. J. Histochem. Cytochem. 63, 494–510. https://doi.org/10.1369/0022155415583534.

Wan, J.-P., Liu, Y., 2012. Recent advances in new multicomponent synthesis of structurally diversified 1,4-dihydropyridines. RSC Adv. 2, 9763–9777. https://doi.org/10.1039/C2RA21406G.

Wang, Y., Wen, X., Zhang, N., Wang, L., Hao, D., Jiang, X., He, G., 2019. Small-molecule compounds target paraptosis to improve cancer therapy. Biomed. Pharmacother. 118. 109203. https://doi.org/10.1016/j.biopha.2019.109203.

World Health Organization (WHO), 2021. Global Health Estimates 2020: Deaths by Cause, Age, Sex, by Country and by Region, 2000-2019. https://www.who.int/data/gho/data/themes/mortality-and-global-health-estimates/ghe-leading-causes-of-death (accessed 4th september 2022).

Ye, R.-R., Tan, C.-P., Lin, Y.-N., Ji, L.-N., Mao, Z.-W., 2015. A phosphorescent rhenium(I) histone deacetylase inhibitor: mitocondrial targeting and paraptosis induction. Chem. Commun. 51, 8353–8356. https://doi.org/10.1039/C5CC02354H.

Yokoi, K., Balachandran, C., Umezawa, M., Tsuchiya, K., Mitrić, A., Aoki, S., 2020. Amphiphilic cationic triscyclometalated iridium(III) complex–peptide hybrids induce paraptosis-like cell death of cancer cells via an intracellular Ca^{2+}-dependent pathway. ACS Omega 5, 6983–7001. https://doi.org/10.1021/acsomega.0c00337.